Cell Reports

CellPress
OPEN ACCESS

Article

Even allocation of benefits stabilizes microbial community engaged in metabolic division of labor

Miaoxiao Wang,[1,2,3,4] Xiaoli Chen,[1,5] Xiaonan Liu,[1] Yuan Fang,[7] Xin Zheng,[7] Ting Huang,[7] Yue-Qin Tang,[4] Martin Ackermann,[2,3] Yong Nie,[1,*] and Xiao-Lei Wu[1,5,6,8,*]

[1]College of Engineering, Peking University, Beijing 100871, China
[2]Department of Environmental Systems Science, ETH Zürich, Zürich, Switzerland
[3]Department of Environmental Microbiology, Eawag, Dübendorf, Switzerland
[4]College of Architecture and Environment, Sichuan University, Chengdu, China
[5]Institute of Ocean Research, Peking University, Beijing 100871, China
[6]Institute of Ecology, Peking University, Beijing 100871, China
[7]School of Resource and Environmental Engineering, Hefei University of Technology, Hefei 230000, China
[8]Lead contact
*Correspondence: nieyong@pku.edu.cn (Y.N.), xiaolei_wu@pku.edu.cn (X.-L.W.)
https://doi.org/10.1016/j.celrep.2022.111410

SUMMARY

Microbial communities execute metabolic pathways to drive global nutrient cycles. Within a community, functionally specialized strains can perform different yet complementary steps within a linear pathway, a phenomenon termed metabolic division of labor (MDOL). However, little is known about how such metabolic behaviors shape microbial communities. Here, we derive a theoretical framework to define the assembly of a community that degrades an organic compound through MDOL. The framework indicates that to ensure community stability, the strains performing the initial steps should hold a growth advantage (*m*) over the "private benefit" (*n*) of the strain performing the last step. The steady-state frequency of the last strain is then determined by the quotient of *n* and *m*. Our experiments show that the framework accurately predicts the assembly of our synthetic consortia that degrade naphthalene through MDOL. Our results provide insights for designing and managing stable microbial systems for metabolic pathway optimization.

INTRODUCTION

Microorganisms colonize all major ecological niches on our planet, from deep terrestrial biosphere miles beneath the land surface (Ian et al., 2003; Jie-Yu et al., 2021; Manuel et al., 2018; Thompson et al., 2017), to the intestinal tracts of mammals (Doron et al., 2021; Flint et al., 2012). In order to thrive in these ever changing habitats, microorganisms have evolved highly sophisticated characteristics to accomplish complex metabolic tasks for biochemical transformations, such as converting a complex substrate into a nutrient suitable for cell growth. As a result, their metabolic activities drive global biogeochemical cycles, and thus profoundly influence the stability of the ecosystems as well as the health of their inhabitants (Paul et al., 2008).

Most of these metabolic tasks are accomplished through long metabolic pathways, which are performed by a single microbial strain. Alternatively, these tasks are divided across different interacting strains, a phenomenon called metabolic division of labor (MDOL) (Emily et al., 2014; Jan-Ulrich et al., 2020; Meghan et al., 2019; Ryan et al., 2018). Several studies have shown that numerous ecologically and environmentally important pathways are accomplished through MDOL. In particular, microbial degradation of complex organic compounds is frequently executed through MDOL. For example, the gut communities digest plant polysaccharides into either sugars or short-chain fatty acids in an MDOL manner, which are then absorbed by the host cells (Hao et al., 2019; Xuefeng et al., 2021). During the Deepwater Horizon oil spill Gulf of Mexico (2010), complete degradation of polycyclic aromatic hydrocarbons (PAHs) required the partitioning of key pathway steps into different bacterial groups (Nina et al., 2016). In more specific cases, syringate can be degraded through MDOL between *Acetobacterium woodii* and *Pelobacter acidigallici* (Bernhard and Norbert, 1982); *Marinobacter* performs only a subset of tasks in phenanthrene degradation, while other marine bacteria perform the remaining steps (Chongyang et al., 2020). As the functioning of a microbial community is determined by its compositional makeup (Emily et al., 2016; Jed, 2009), it is critical to understand the factors that determine the stability and the structure of microbial communities engaged in MDOL (simplified as MDOL communities thereafter).

Inspired by natural MDOL communities, numerous studies have recently engineered synthetic communities engaged in MDOL for the removal of organic pollutants (Pablo et al., 2020). For instance, one study engineered a defined consortium composed of an *Escherichia coli* strain and a *Pseudomonas*

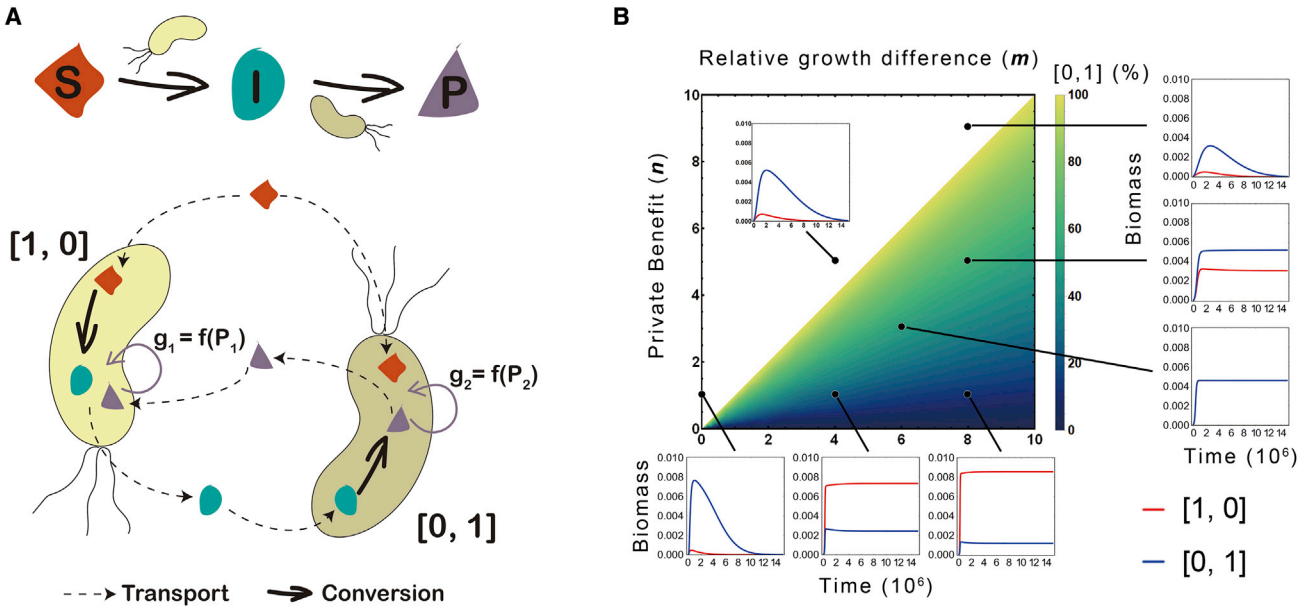

Figure 1. Assembly rule of microbial community engaged in two-step MDOL

(A) Schematic diagram showing the assumptions of our basic model. We assumed a conceptualized organic substrate (S) could be degraded into an intermediate metabolite (I) by a strain [1, 0], then to a final product (P) by the other strain [0, 1]. All the reactions occurred intracellularly, while S, I, and P passively diffused across the cell membrane. Importantly, the growth of both strains is dependent on the intracellular concentration of P, which is the sole limiting resource of this system.

(B) The density map indicates the assembly rule of the two-step MDOL community. The value of privatization benefit (n) and relative growth advantage (m) determines whether [1, 0] and [0, 1] can stably co-exist (shown by the colorized space), as well as the relative abundance of [0, 1] in the stable community (shown by the color gradient). The corresponding curve graph illustrates the community dynamics of the community under six specific n and m combinations. In these simulations, the growing cost of the strain [0,1] (c_2) was adjusted to modify m, and the diffusion coefficient of the final product (γ_p) was adjusted to modify n. The default values listed in Table S2 were assigned for other parameters.

aeruginosa strain for phenanthrene bio-removal via MDOL (Xiaoqiang et al., 2019). Another study investigated how MDOL in a consortium composed of *Stenotrophomonas* and *Advenella* affects phenol biodegradation (Chang-Mei et al., 2020). These studies tested mainly whether MDOL enhances the efficiency of biodegradation compared with relevant monocultures composed of single species. However, specific strains may not be able to stably co-exist in an artificial co-culture system (Bruce and Korneel, 2012; David, 2012; Jonathan et al., 2017; Lori et al., 2019), resulting in the collapse of the community. To guide the rational engineering of stable MDOL communities, it is essential to build quantitative rules that reliably predict whether a specific combination of strains can successfully assemble into a robust MDOL system.

One of our recent works was performed to define such quantitative rules (Miaoxiao et al., 2022). We found that the properties of the substrate, such as its concentration and toxicity, largely affected the assembly of the MDOL community. Nevertheless, a number of biotic and abiotic factors, such as the metabolic burden of each strain (the energy cost of performing its specific functional step within the pathway), mass transfer rate, as well as the toxicity of substrate or intermediates, may also contribute to the assembly of MDOL community. A general rule combining all these factors remains absent, rendering any prediction of how MDOL communities assemble challenging.

Here, we addressed this knowledge gap using a bottom-up approach. We first built an ordinary differential equation (ODE) model to formalize a rule that predicted how an MDOL community assembled. We next tested this rule by performing *in vitro* assays using a series of engineered synthetic consortia implementing naphthalene degradation through two- or multi-step MDOL.

RESULTS

Model framework for a community performing two-step MDOL

To describe the dynamics of a community engaged in metabolic division of labor (MDOL community), we conceptualized the degradation of an organic compound by a microbial consortium composed of two strains using a simple mathematical model (Figure 1A). In this consortium, the first strain (named [1, 0]) expresses an enzyme (E1) to catalyze the conversion of an organic substrate (S) into an intermediate metabolite (I), while the second strain (named [0, 1]) performs the subsequent conversion of I to a final product (P) by expressing another enzyme (E2). In the basic model, transport of S, I, and P across the cell membrane was assumed to occur via passive diffusion mediated by coefficients γ_s, γ_i, and γ_p. Following these assumptions, we formulated the dynamics of intracellular and extracellular concentrations of I

and P by using seven ordinary differential equations (Equations 8, 9, 10, 11, 12, and 13 in STAR Methods). Consistent with our previous hypotheses and observations (Miaoxiao et al., 2022), we next assumed that P, which was produced by the second strain, was the sole resource for the growth of both strains, while S and I cannot be directly assimilated as a carbon source. Consequently, [0, 1] possesses preferential access to the final product (P), resulting in a "private benefit" derived from product privatization (Figure 1A). Details about the model construction are described in STAR Methods, as well as supplemental information (see the resource availability section in STAR Methods). Meanings of the variables and parameters of the model are listed in Tables S1 and S2.

Deriving the criterion for maintaining a stable two-step MDOL community

To derive the criterion defining the stability of a two-step MDOL community, we solved steady-state expressions of Equations 8, 9, 10, 11, 12, 13, 14, 15, 16, and 17. We obtained a simple formula, which suggests that if the steady state of a two-step MDOL community exists, the relative abundance of [0, 1] ($R_{[0,1]}$) should follow:

$$R_{[0,1]} = \frac{n}{m}. \qquad \text{(Equation 1)}$$

Here, $n = lg_1/\gamma_p$, reflecting whether the supply of P (produced and secreted by [0, 1]) is sufficient for the growth of [1, 0] (defined as the "product demand gap" for [1, 0]). For example, a lower "product demand gap" of [1, 0] suggests that [0, 1] privatized more P and share less to [1, 0], thus n also indicates the "private benefit" of [0, 1] derived from the product privatization. $m = \left(\frac{c_1 l g_1 y_1}{d_1} - \frac{c_2 l g_2 y_2}{d_2}\right) \Big/ \frac{c_2 l g_2 y_2}{d_2}$ is the normalized difference between the inherent growth rates of the two strains. Importantly, because $R_{[0,1]}$ ranges from 0 to 1, we derived a prerequisite defining the conditions when the two strains were able to stably co-exist:

$$0 < n < m\,. \qquad \text{(Equation 2)}$$

We offer two intuitive explanations for Equation 2. First, the requirement $m > 0$ suggests that [1, 0] must hold a growth advantage than [0, 1]. Second, the requirement $n < m$ indicates that the "private benefit" of [0, 1] must be lower than the growth advantage of [1, 0]. We visualized Equations 1 and 2 by a two-dimensional density map. As shown in Figure 1B, the MDOL community assembled to a steady state only when the values of n and m fell inside the range defined by Equation 2, and the community structure at the steady state can be directly assessed by Equation 1. We next performed additional analyses to test whether other parameters that are not included in n and m also affect the proposed rule (Figure S1). Our results indicated that the stability of the MDOL community also requires the speed of the first reaction (a_1; Figures S1A and S1B) and the initial biomass ($x_{i,0}$; Figures S1K–S1M) to reach the critical thresholds. We also linked the stability and structure of an MDOL community with its function (the degradation ability of the substrate). As shown in Figures S1N and S1O, the MDOL community shows higher degradation ability when it meets our proposed condition defining the stability, and the degradation ability of the steady-state community was positively correlated with the steady-state frequency of [1, 0].

In summary, our mathematical model defined a rule that defines the condition when the two strains in an MDOL community can stably co-exist, namely, when the strain [1, 0] possesses a growth advantage that outweighs the "private benefit" of the strain [0, 1] (Equation 2). When the steady state exists, this rule also provides a prediction of the steady-state community structure (Equation 1).

Stability of MDOL in response to changing metabolic conditions

For simplicity, our basic model ignored many complex pathway mechanisms. For example, mass transport across the cell membrane can be mediated by an active transporter protein (Nicole and Marlon, 2014) (Figures 2A, S2A, and S2B). In addition, both metabolic reactions involved in an MDOL pathway might be performed extracellularly (Blair et al., 2021) (Figures 2B and S2D). Moreover, the intermediates of an MDOL pathway can be converted to chemicals unavailable to microorganisms via spontaneous reactions (Greg et al., 2018; Shalini et al., 2014) (Figure 2C; Figure S3A). Furthermore, metabolic by-products may be generated from the conversion from S to I (Debajyoti et al., 2016; Rafael et al., 1999; Shalini et al., 2014) (Figures 2D and S3C), which may facilitate the growth of [1, 0]. Finally, toxic effects of substrate (Graham and Eugene, 2007; Park et al., 2004), intermediates (Graham and Eugene, 2007; Mariana et al., 2009; Muoz et al., 2007; Park et al., 2004), and final product (Aiba et al., 2000; Alejandro, 1983) are common during microbial degradation of organic compounds (Figures 2E–2G, S4A, S4C, and S5A). Therefore, we modified the basic form of our model to address how these additional mechanisms affect the assembly of an MDOL community:

1. The MDOL community becomes more likely to reach a steady state when we assumed that the final product (P) is actively taken up by [1, 0], or is actively secreted by [0, 1] (Figure 2A; Figure S2C).
2. When only the first metabolic step is catalyzed extracellularly, the basic prediction of our rule remains unchanged (Figures 2B and S2D). However, once the second metabolic step is performed extracellularly, the rule change considerably. Our results indicated that the co-existence of the two strains requires an additional condition defined by Equation S2.35. In addition, the structure of the stable MDOL community is strongly dependent on the initial abundance of the two strains (Figures S2E and S2F).
3. When we included the spontaneous conversion of I, P, or both in our model, we found that the points defining the stability of an MDOL community were restricted to a smaller part of the parameter space (Figures 2C and S3B).
4. We next assumed that the conversion of S to I can generate a by-product that can be assimilated by [1, 0] as a carbon source (Figures 2D and S3C). Under this condition, the "private benefit" of [0, 1] was counteracted by

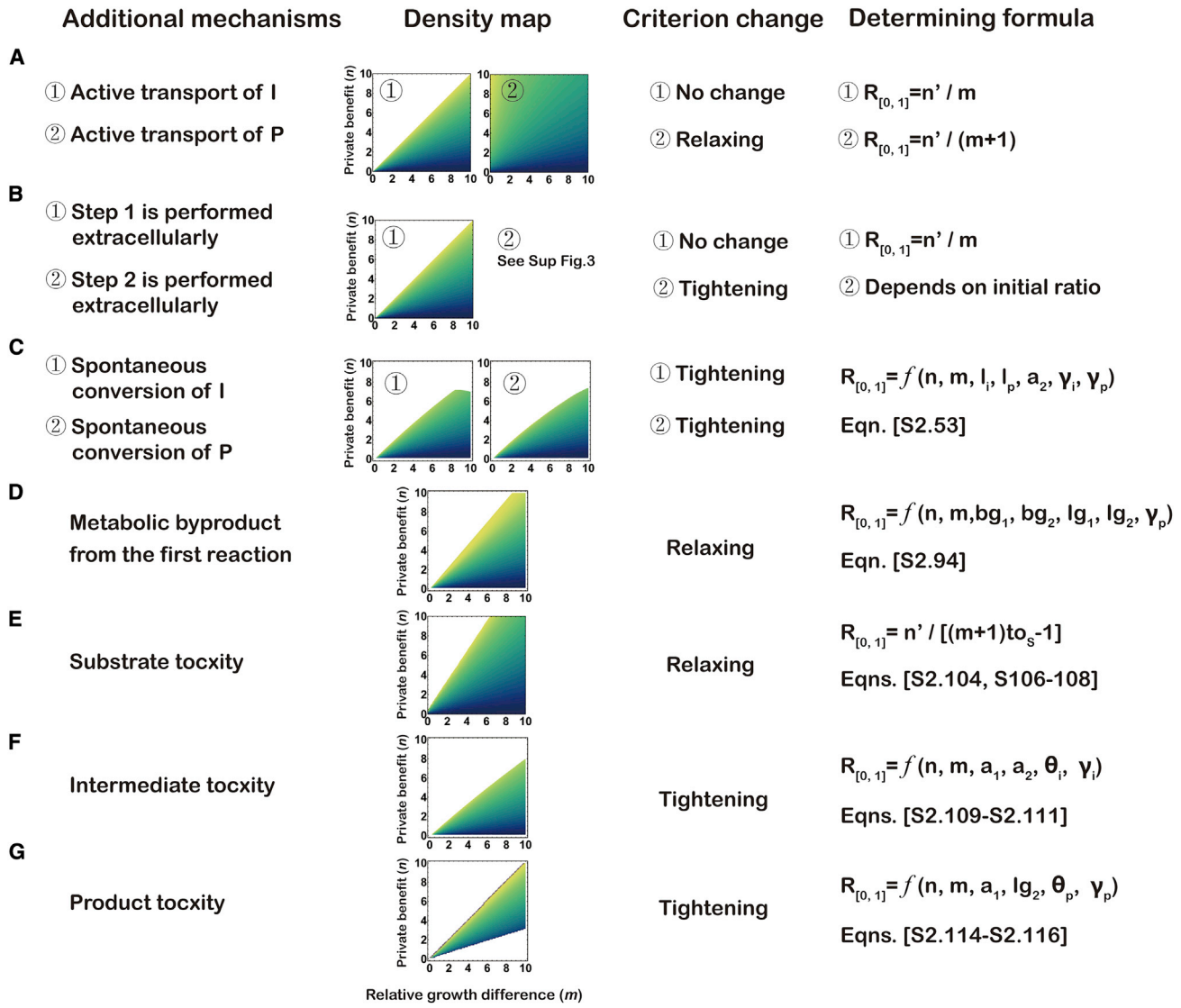

Figure 2. Additional pathway mechanisms influence the assembly of the two-step MDOL community

(A–G). Seven additional pathway mechanisms were tested: (A) different configurations for the transport of the intermediate and product (Figures S2A–S2C); (B) alternative or both metabolic reactions occurring in the extracellular space (Figures S2D–S2F); (C) presence of abiotic conversion of intermediate and product (Figures S3A and S3B); (D) presence of by-product generated from the first reaction (Figures S3C and S3D); (E) presence of biotoxicity of the substrate (Figures S4A and S4B); (F) presence of biotoxicity of intermediate (Figures S4C–S4F); and (G) presence of biotoxicity of the end product (Figure S5). First column: descriptions of the specific pathway mechanisms. Second column: representative density maps shows how the additional pathway mechanisms change the assembly rules. Third column: summary of how the additional pathway mechanisms change the criterion for the stability of the community. "Tightening" means that the size of the parameter space required for stability decreases, thus the two-step MDOL community becomes more difficult to maintain stability. In contrast, "relaxing" means that the size of the parameter space required for stability increases, thus the two-step MDOL community becomes easier to maintain stability. Fourth column: summary of the derived formulas that determine the assembly of two-step MDOL community at steady state in each scenario. For simplicity, the key influencing factors of the scenarios in (C), (D), (F), and (G) are listed. Detailed expressions of these formulas are available are described in the publicly available supplementary file (Mendeley Data, https://doi.org/10.17632/87ctyv6chg.1), of which the tracking number is listed.

the by-product, strongly favoring [1, 0] and the co-existence of the two strains (Figure S3D).

5 .We then tested the toxic effects of S, I, and P on the community assembly (Figures 2E–2G, S4, and S5). Although substrate toxicity neutralizes the "private benefit" of [0, 1] (Figure S4B), the presence of intermediates toxicity offers an additional benefit to [0, 1], which restricts the points of stability to a smaller part of the parameter space (Figures S4D–S4F).

Experimentally testing the rules of community assembly and stability achieved by synthetic microbial consortia

To experimentally test our proposed rule, we engineered three synthetic consortia that degrade naphthalene via two-step

MDOL. In these systems, a first *Pseudomonas stutzeri* strain converts naphthalene into its intermediate (i.e., 1,2-hydroxynaphthalene, salicylate, or catechol), which can diffuse between the cytoplasm and the external environment (Isabel et al., 2012; Rafael et al., 2000) but cannot be directly used as the carbon source to support bacterial growth. The second strain possesses the ability to degrade the intermediate to the final products (pyruvate and acetyl-coenzyme A [CoA]), which are then partially and passively secreted to the environment and utilized by the consortia as the limiting carbon source (Figures 3A, S6A, and S6E). To predict the assembly of these synthetic ecosystems, we modified our basic model to include specific pathway mechanisms corresponding to these consortia. For instance, the toxic effects of naphthalene, as well as the three intermediates, were experimental measured and introduced as the model parameters. The spontaneous conversions of 1,2-hydroxynaphthalene and catechol were included according to previously reported reaction kinetics (Greg et al., 2018). Accordingly, we mathematically derived the quantitative criteria to predict the stability and assembly of our synthetic consortia (Figures 3B, S6B, and S6F).

Using the consortium composed of strain AN1000 and strain AN0111 (Figure 3A) as an example, our modeling analyses suggest that the points defining the stability of this consortium were located in a larger parameter space compared with those in our basic rule (Figure 3B compared with Figure 1B), mainly because of the toxic effect of naphthalene. To test the predictive power of our theoretical criterion, we cultured the consortium using naphthalene as the sole carbon source. As the two strains exhibited a similar inherent growth rate (meaning $m = -0.031$), the consortia were found to be ecologically unstable (Figure S7A), consistent with the prediction of our model.

To obtain a stable MDOL community, we set out to modify the m value of this system according to our theoretical framework. To this end, we introduced two toxic genes to control the growth of the strain AN0111, that is, *ccdB* and *phiX174 E*. The toxin CcdB inhibits the activity of DNA gyrase, causing the breakage of plasmid and chromosomal DNA, and thus deactivates the cells (Minh-Hoa et al., 2005). The phiX174 E is the lysis protein of bacteriophage phiX174, which disrupts bacterial peptidoglycan biosynthesis by inhibiting the phospho-MurNAc-pentapeptide translocase (MraY) (Henrich et al., 1982). We engineered two genetic modules, in which the expression of *ccdB* or *phiX174 E*, is controllably induced by rhamnose (Figure 3A). Then, we introduced the ccdB module into the cells of strain AN0111, generating strain AN0111ccdB. Similarly, the phiX174 E module was knocked in to generate strain AN0111x174. Quantitatively fitting analysis suggests that the death rate of these strains (d_2) is linearly correlated with logarithmic forms of the rhamnose concentration. As m is directly associated with d_2 (according to the definition of m), the experimental modifications of m can be fulfilled by setting up the rhamnose concentration. We co-cultured the modified strain AN0111 with strain AN1000, mimicking the community dynamics with a given n value of 2.53 (estimated by the experimental measurement of lg divided by the previously reported value of γ_p (Chi Kyu et al., 2006)), and a gradient of m values (Figure 3B, blue line). The results showed that when the value of m is lower than the threshold at which our models predict that the two strains fail to stably co-exist (that is when $m < 1.7$), our synthetic consortium collapsed (Figures 3C, 3D, S7D, and S7G). In contrast, when m was set over the threshold, the consortium stabilized (Figures 3C and 3D), and the two strains co-existed for at least three growth cycles (Figures S7D and S7G). Further analyses showed that our mathematical modeling accurately predicted the steady-state frequency of strain AN0111 in the consortium ($R^2 = 0.927$; Figure 3E).

We then tested our proposed rule using two additional synthetic consortia degrading naphthalene. One consortium is composed of strains AN1100 (converting naphthalene to salicylate) and AN0011 (further degrading salicylate to pyruvate; Figure S6A), and the other is composed of strains AN1110 (converting naphthalene to catechol) and AN0001 (further degrading catechol to pyruvate; Figure S6E). In both cases, pyruvate was produced from the first reaction as a by-product. Our models predicted that the points defining the stability of these two consortia were located in a larger parameter space than those in the consortium composed of AN1000 and AN0111 (Figures S6B and S6F compared with Figure S3B). These predictions were verified by our co-culture experiments (Figures 3F, 3G, S6, and S7). Together, these results indicated that our mathematical framework accurately predicts the assembly of our consortia, and thus can be a reliable guide for the construction of stable synthetic consortia engaged in MDOL.

Assembly and stability of a community performing multi-step MDOL

We next investigated the assembly rule of a community executing multi-step MDOL, a situation in which a long metabolic pathway is distributed among more than two strains in microbial communities (Jones et al., 2017). To this end, we expanded our basic model (based on 2-step MDOL) to build a mathematical framework conceptualizing the dynamics of an ***N***-step MDOL community (Figure 4A; Equations 18, 19, 20, 21, 22, and 23 in STAR Methods). We derived a formula on the basis of the analyses of these equations, which defines the steady-state frequency of the strain that performs the last step in a community performing N-step MDOL:

$$R_N = \sqrt[h]{\frac{1}{N-1}\sum_{k=1}^{N-1}\left(\frac{n_k}{m_k}\right)^h}. \qquad \text{(Equation 3)}$$

Here, $n_k = lg_k / \gamma_p$ represents the "product demand gap" of the kth strain, reflecting the relative "private benefit" of the strain performing the last step (simplified as the last strain thereafter; Figure 4A) against the kth strain, while $m = \left(\frac{c_k lg_k y_k}{d_k} - \frac{c_N lg_N y_N}{d_N}\right) \Big/ \frac{c_N lg_N y_N}{d_N}$ represents the normalized difference between the inherent growth rates of the kth strain and the last strain; h is a fitted exponent affected by the environmental capacity and reaction speed of each metabolic step. Our analysis also identified the two prerequisites that define the co-existence of the strains involved in these complex systems:

$$\frac{n_1+1}{m_1+1} = \frac{n_2+1}{m_2+1} = \ldots = \frac{n_k+1}{m_k+1} = \ldots = \frac{n_{N-1}+1}{m_{N-1}+1} = ra. \qquad \text{(Equation 4)}$$

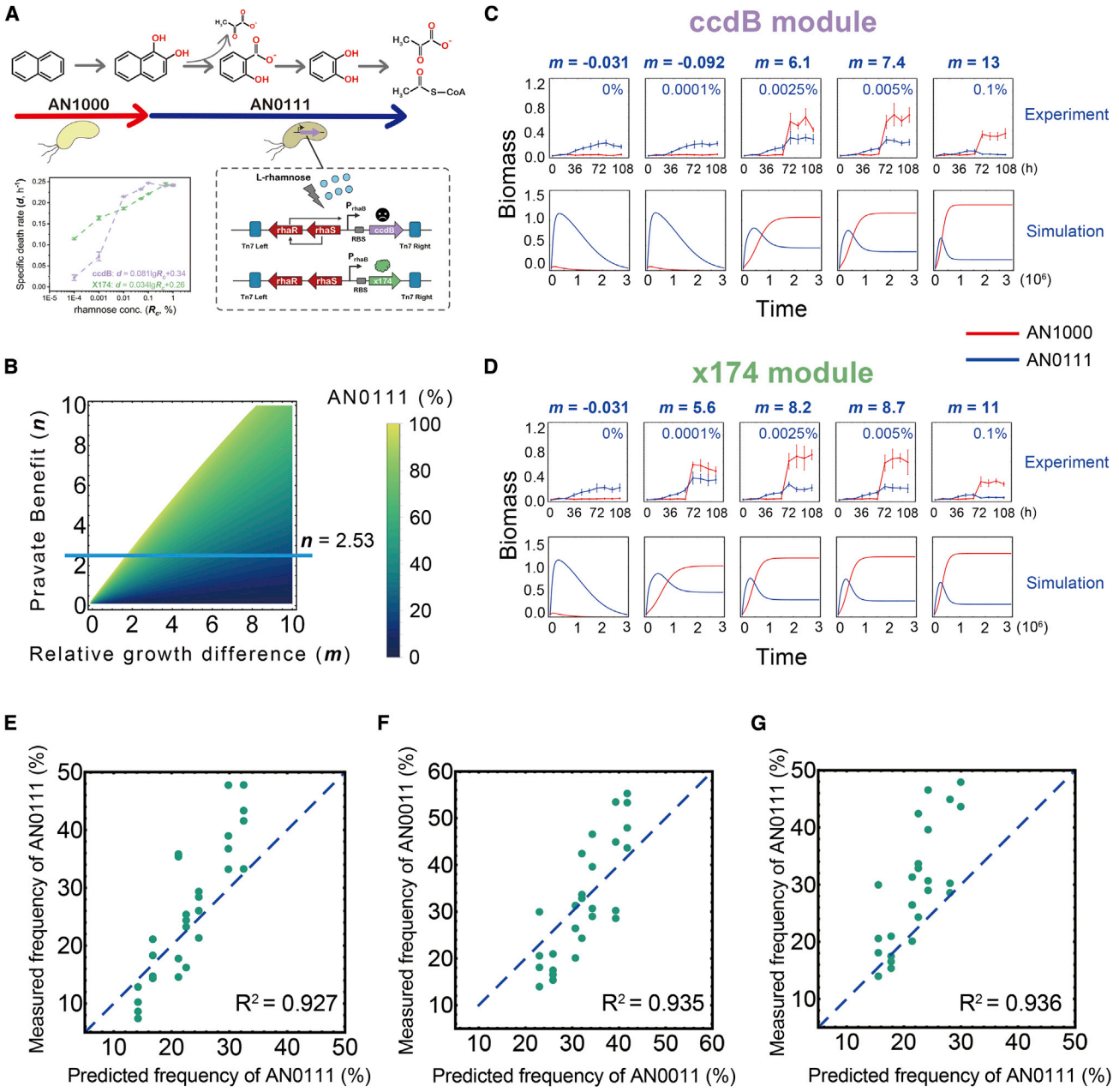

Figure 3. Dynamics of the synthetic community composed of *P. stutzeri* AN1000 and *P. stutzeri* AN0111ccdB

(A) Schematic diagram of the construction of the synthetic consortium. To experimentally modify the *m* value, two genetic modules were introduced into strain *P. stutzeri* AN0111, generating *P. stutzeri* AN0111ccdB and *P. stutzeri* AN0111x174, in which the expression of a toxic protein, CcdB or phiX174 E, are controllably induced by rhamnose. Therefore, the death rate of the modified strain can be quantitatively modulated by adjusting rhamnose concentration, as shown in the left plot.

(B) Predicting the assembly of the synthetic community by mathematical modeling. The density map shows the parameter space in which the community can maintain (the colorized space), as well as the relative abundance of *P. stutzeri* AN0111ccdB or *P. stutzeri* AN0111x174 in the stable community (the color gradient). The blue line suggests that in our synthetic community $n = 2.53$, which is the region we performed experimental verification.

(C and D) The dynamics of the synthetic community composed of *P. stutzeri* AN1000 and *P. stutzeri* AN0111ccdB (C) or *P. stutzeri* AN1000 and *P. stutzeri* AN0111x174 (D) from co-culture experiments and mathematical modeling under different rhamnose concentrations (that is, a gradient of *m* values). To measure their relative abundance, the strain performing the first step was labeled with MCherry, while the other strain was labeled with EGFP. Four independent replicates were performed for each condition. The error bar indicates the standard error of the replicates.

(E–G) Testing the predicting power of our mathematical frameworks. The experimentally measured frequency of the last strains of all the three synthetic communities performing two-step MDOL is compared with the predicted frequency from our mathematical framework. The data are collected in dilution-transfer experiments (Figure S7), and the values of relative abundance at the end of the third transfer were recorded. Each green dot indicates one experimental replicate. The blue dashed line indicates the line in which the experimental results and predicted results are identical. The adjusted R^2 value is acquired from statistical fit using the LinearModelfit function of Wolfram Mathematica (version 12.0).

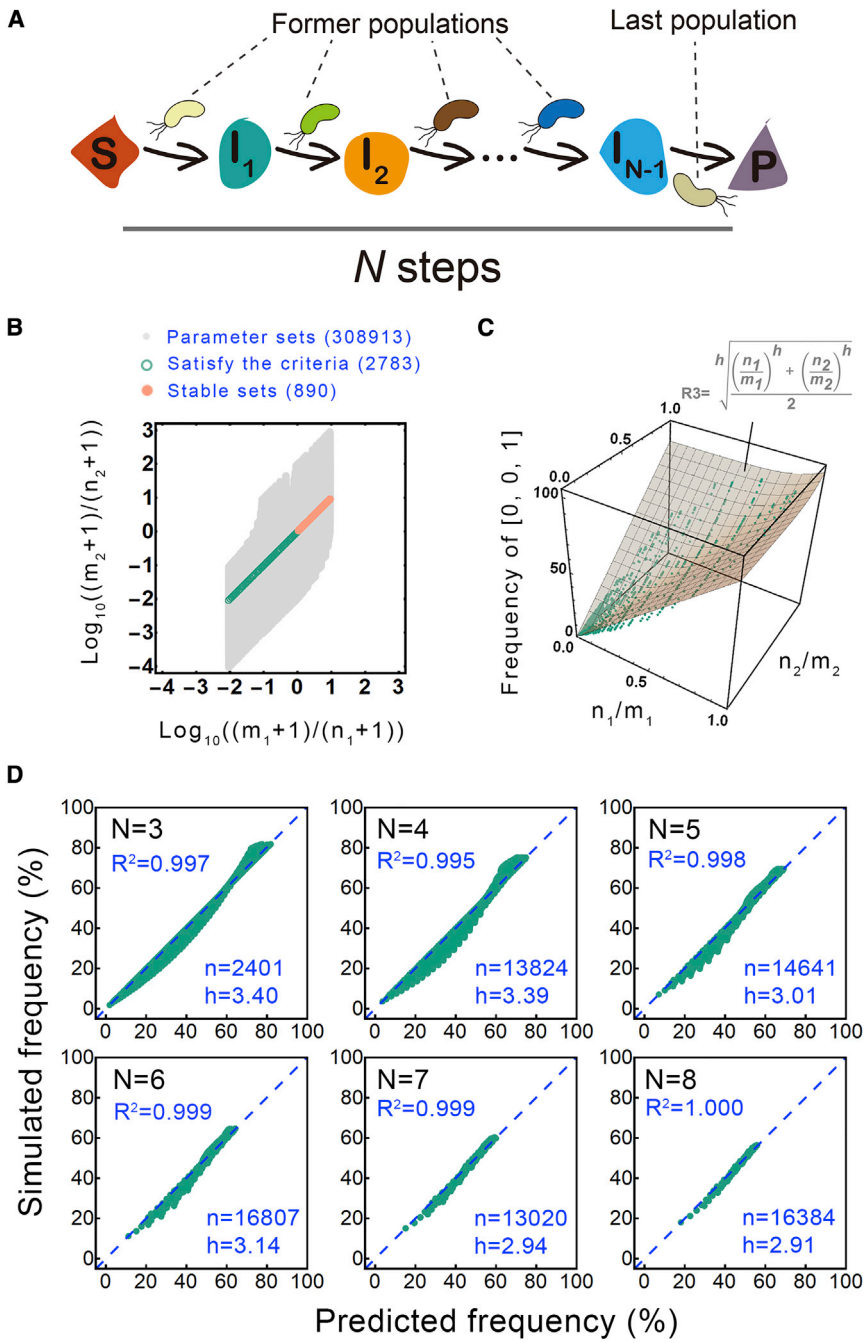

Figure 4. Assembly rule of microbial community engaged in multi-step MDOL

(A) A schematic diagram shows the assumptions of the model regarding the assembly of a multi-step MDOL community. We assumed a conceptualized organic substrate (S) was degraded into the end product (P) through $N - 1$ intermediates, and the jth intermediate was labeled with I_j. Each reaction was carried out by one strain and occurred intracellularly.

(B) The first condition required for the stability of the community engaged in three-step MDOL. The graph depicts the distribution of 308,913 designed parameter sets to test the first condition required for the stability of a three-step MDOL community. The gray dots indicate the distribution of all the sets; The green dots and orange dots indicate the parameter sets that satisfy the proposed condition defined by Equation 4; the orange dots indicate the parameter sets that lead to stable community dynamics.

(C) Assembly rule of microbial community engaged in three-step MDOL. The relationship between the relative abundance of [0, 0, 1] and the ratio n_1/m_1 and n_2/m_2 in 890 simulated steady-state communities. Each dot shows the relative abundance of [0, 0, 1] obtained by the simulation parameterized with the corresponding value set. The surface diagram shows the distribution of the relative abundance of [0, 0, 1] predicted by Equation 3.

(D) The linear correlation between the relative abundances of the last strain (R_N) in those stable N-step MDOL communities predicted by Equation 3 and those abundances obtained by simulations. Comparisons of three- to eight-step MDOL communities are shown (meaning N = 3∼8). The dashed lines show the fitted linear correlation curve. N is the number of the simulations included, and h is the optimal mean-square index h. Details of these simulations are described in are described in the publicly available supplementary file (Mendeley Data, https://doi.org/10.17632/87ctyv6chg.1). The adjusted R^2 value is acquired from statistical fit using the LinearModelfit function of Wolfram Mathematica (version 12.0).

$$0 < \frac{n_k}{m_k} < 1. \qquad \text{(Equation 5)}$$

Here, *ra* represents the relative inherent growth rates of the strain performing the last step to the *k*th strain performing the *kth* step.

Using three-step MDOL community as an example (the three strains performing the first to third steps were named [1, 0, 0], [0, 1, 0], [0, 0, 1], respectively), our simulations showed that the three strains co-exist only when the *ra* value of [1, 0, 0] equals that of [0, 1, 0] (prerequisite defined by Equation 4; Figure 4B) and the values of n_k/m_k belong to the range defined by Equation 5 (Figure 4C). This result suggests that an MDOL community can maintain stability if the strains performing the initial steps (the steps except for the last step; Figure 4A) exhibit comparable inherent growth rates (Equation 4). In addition, these strains are required to maintain a growth advantage that outweighs the "private benefit" of the last strain (Equation 5). Under steady-state conditions, we successfully estimated the frequencies of [0, 0, 1] using Equation 3 (Figure 4C). Importantly, Equation 3 can be expanded to estimate the results of mathematical simulations considering an MDOL community with more steps (Figure 4D; up to n = 8). Remarkably, the rule

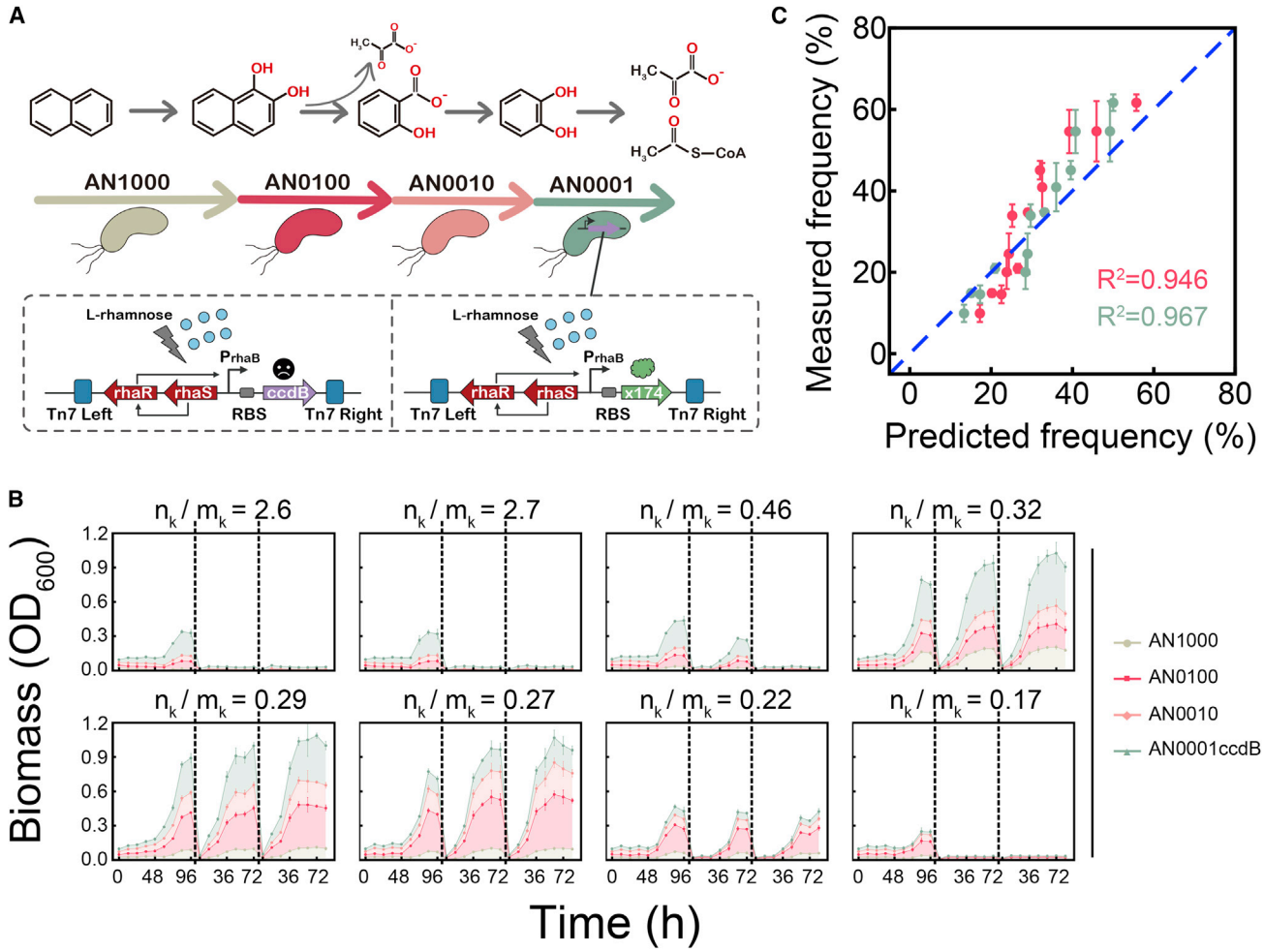

Figure 5. Dynamics of the four-step synthetic community

(A) Schematic diagram of the construction of the synthetic community. To experimentally modify m_k, strain *P. stutzeri* AN0001ccdB or *P. stutzeri* AN0001x174 was used.

(B) The dynamics of the synthetic community composed of *P. stutzeri* AN1000, *P. stutzeri* AN0100, *P. stutzeri* AN0010, and *P. stutzeri* AN0001ccdB from co-culture experiments under a gradient of n_k/m_k value conditions (i.e., using a medium with different rhamnose concentrations). The cultures were diluted by a factor of 20 after 96 or 72h of culturing (indicated by the dashed line) and transferred into a new fresh medium. To measure their relative abundances, strain *P. stutzeri* AN1000 was labeled with ECFP, strain *P. stutzeri* AN0100 was labeled with DsRed, strain *P. stutzeri* AN0010 was labeled with mBeRFP, and strain *P. stutzeri* AN0001ccdB was labeled with EGFP. The dynamics of the community composed of *P. stutzeri* AN1000, *P. stutzeri* AN0100, *P. stutzeri* AN0010, and *P. stutzeri* AN0001x174 are shown in Figure S8C. Three independent replicates were performed for each condition. The error bar indicates the standard error of the replicates.

(C) Predicting the relative abundance of the last strains (that is, *P. stutzeri* AN0001ccdB or strain *P. stutzeri* AN0001x174) by mathematical modeling. The experimental results are summarized from those stable communities shown in (B) and Figure S8C, in which the values of relative abundance at the endpoint of the third transfer were recorded. The red dots show the results calculated by the Equation 3, while the green dots show the results predicted from the simulations considering the specific pathway mechanisms of naphthalene degradation. The model is described detailly in the publicly available supplementary file (Mendeley Data, https://doi.org/10.17632/87ctyv6chg.1). The adjusted R^2 value is acquired from statistical fit using the LinearModelfit function of Wolfram Mathematica (version 12.0). The error bar indicates the standard error of the experimental replicates.

we proposed about the assembly of a two-step MDOL community is a specific case of this rule (when set $n = 2$ in Equation 3, we obtain Equation 1). Together, we successfully expanded our mathematical framework to estimate the assembly of the multi-step MDOL community.

To experimentally verify our expanded rule, we separated the naphthalene degradation pathway into four steps and engineered four *P. stutzeri* strains (*P. stutzeri* AN1000, *P. stutzeri* AN0100, *P. stutzeri* AN0010, and *P. stutzeri* AN0001) that possess similar inherent growth rates (Figure S8A) and execute complementary metabolic reactions to degrade naphthalene by exchanging the three intermediates (Figure 5A). The limiting carbon source of this consortium was mostly supplied by the last strain, *P. stutzeri* AN0001, which converts catechol to pyruvate and acetyl-CoA that can be assimilated (Figure 5A).

We next cultured this consortium using naphthalene as the sole carbon source. Because the inherent growth rates of strains AN0001, AN1000, AN0100, and AN0010 are nearly identical, meaning $m_k \approx 0$, the community showed signs of collapse (Figure S8B), consistent with our basic predictions (Equation 5). To generate a stable synthetic consortium, we applied a similar strategy to that used in stabilizing our two-step MDOL consortia: experimentally modifying the value of m_k by co-culturing the consortia containing a *P. stutzeri* AN0001 strain integrated with the CcdB or phiX174 E module (named *P. stutzeri* AN0001*). In these experiments, we found that the consortia maintained stability when the values of n_k/m_k were present within a suitable range (Figures 5B and S8C) given by Equation 5. In addition, as shown in Figure 5C (red dots), Equation 3 accurately predicts the steady-state frequency of strain *P. stutzeri* AN0001* ($R^2 = 0.946$). Moreover, although the assembly of this synthetic consortium may be affected by various factors, including the by-product generated from the initial steps, spontaneous conversion of intermediates, as well as toxic effects of the metabolites, we found that the model excluding these factors (Figure 5C; red dots) enables similarly accurate prediction of the community assembly to the model considering these factors (Figure 5C, green dots). However, whether these factors actually affect the community assembly requires further tested. Taken together, these results demonstrated that our theoretical framework can be expanded to multi-step MDOL communities, thus greatly contributing to a more detailed understanding of their assembly.

The effects of the initial frequency on the assembly

The structure of the founding community is a key factor that governs the assembly of a community (Jonathan, 2003; Tadashi, 2015). For example, microbial communities can display alternative assembly trajectories dependent on the initial frequency of different members (Eulyn et al., 2017; Ori et al., 2020). Nevertheless, one recent study observed that a synthetic community composed of two strains that perform two-step MDOL converges to a stable state regardless of their initial frequency (Robin and Dani, 2017). We thus set out to test whether this characteristic can be captured by our quantitative framework, as well as whether a community engaged in multi-step MDOL also remains robust to the changing initial frequency.

For the two-step MDOL community, our simulations indicated that the rule given by Equation 2 still accurately predicts whether the two strains stably co-exist (Figure S9A). If a community maintains stability, our modeling results suggested that the steady-state ratio of the two strains involved converged to the same value that can be quantitatively predicted by Equation 1 (Figures S9A and S9B). Similar results were observed in our verification experiments (Figures S9C–S9E). These results suggest that the assembly of the two-step MDOL community is independent of the initial ratio of the two strains involved.

We then set out to test whether the assembly of a multi-step MDOL community was influenced by the initial frequency of the different members involved. As shown in Figure S10, when one of the strains dominated the initial community, the parameter space for the stable co-existence decreased, suggesting that these extreme initial conditions considerably destabilize the community. If the community maintains stability, the frequency of one strain performing the initial steps was significantly positively correlated with its initial frequency (Figures S11A, S11D, and S11G) and was determined largely by the proportion of its initial abundance accounting for the total initial abundance of all the former strains (Figures S11B, S11E, and S11H). We defined this proportion as σ_k:

$$\sigma_k = \frac{x_k^0}{\sum_{k=1}^{N-1} x_k^0}. \qquad \text{(Equation 6)}$$

Here, x_k^0 represents the initial biomass of the kth strain ($k = 1 \sim N$). Moreover, the frequency of the last strain in the steady-state community remained unchanged despite changing initial conditions (Figures S10A, S10B, S11A, S11D, and S11G), but this frequency did not match well with the prediction of Equation 3. This result suggests that the steady-state frequency of the last strain is affected by the structure of the founding community. To quantitatively describe this characteristic, we added σ_k as a weight to the original formula Equation 3, generating a novel formula:

$$R_N = \sqrt[h]{\sum_{k=1}^{N-1} \sigma_k \left(\frac{n_k}{m_k}\right)^h}. \qquad \text{(Equation 7)}$$

Our simulations and fitting analysis indicated that Equation 7 predicted the frequency of the last strain more accurately than Equation 3 (Figures S10A, S10B, S11C, S11F, and S11I). These mathematical predictions were then verified in our synthetic consortium engaged in four-step MDOL (Figures 6B–6D and S8D–S8F). Together, these results suggested that the initial strain ratio, especially the initial ratio of the former strains, plays a critical role in governing the assembly of a multi-step MDOL community.

DISCUSSION

Here, we proposed a simple rule to predict the assembly of microbial communities engaged in metabolic division of labor (MDOL community) using a mathematical model. This rule was verified by experimental work using synthetic microbial consortia. Our rule demonstrates that the stability and assembly of an MDOL community are mostly determined by how benefits are allocated among the community members.

Importantly, our rule is built on one basic assumption derived from most organic compound degradation pathways, that is, the final product of an MDOL pathway is the sole carbon source for all the strains involved in the community. This feature offered a "private benefit" to the last strain, which destabilizes MDOL communities and challenges the development of such communities. This phenomenon has been observed in many MDOL communities. For instance, one study engineered a dual-species consortium for removal of the insecticide parathion, in which an *Escherichia coli* strain hydrolyzes parathion, yielding two intermediates including *p*-nitrophenol, while another *Pseudomonas putida* strain metabolizes *p*-nitrophenol (Gilbert et al., 2003). That study revealed that *P. putida* largely dominated the final

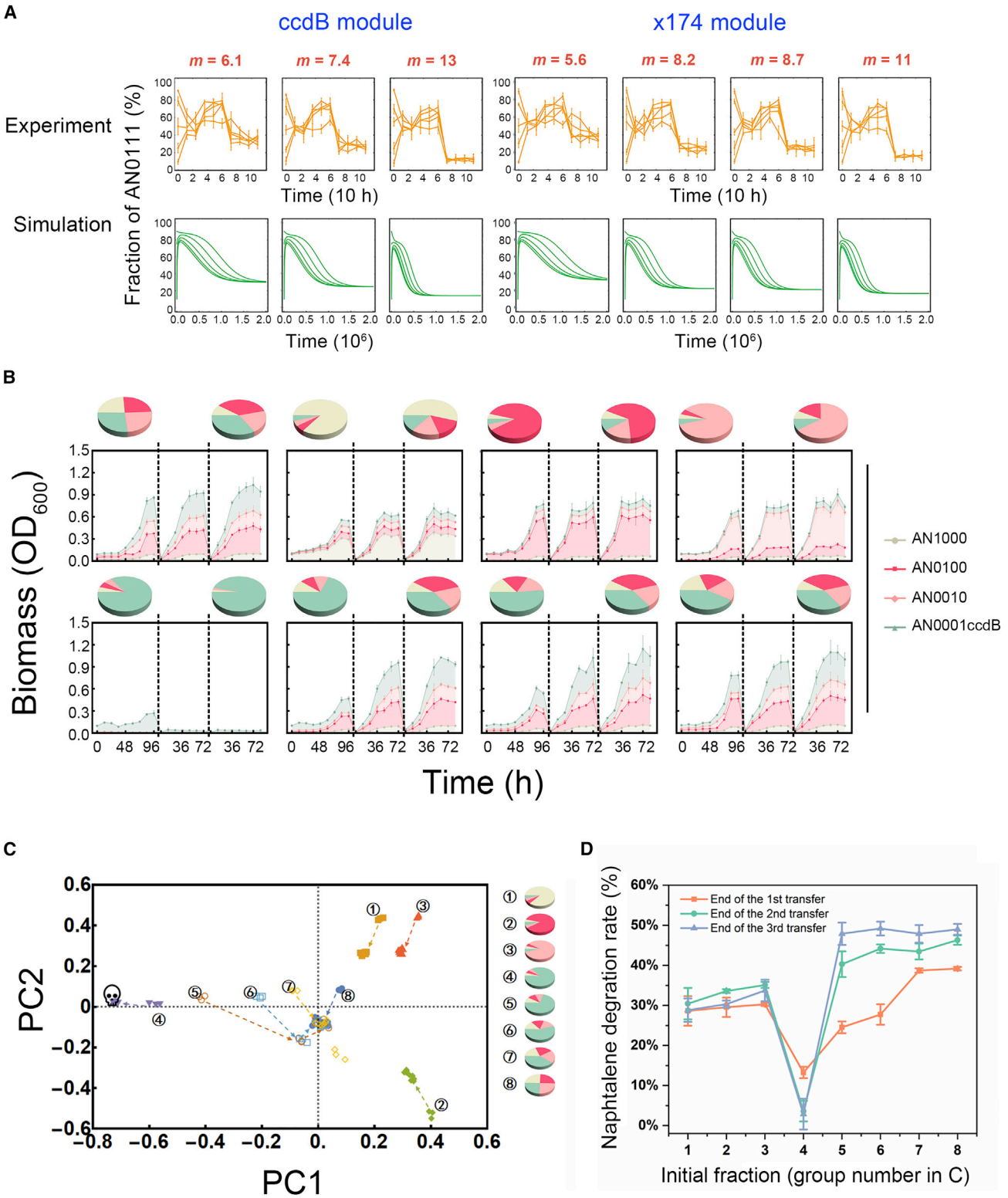

Figure 6. Effects of initial strain ratio on the assembly rule of microbial community engaged in MDOL

(A) The assembly rule of the two-step MDOL community is independent of the changing initial strain ratio. Culture experiments and mathematical modeling of the community composed of *P. stutzeri* AN1000 and *P. stutzeri* AN0111ccdB (or *P. stutzeri* AN0111x174) were performed by setting seven different *m* values, as well

(legend continued on next page)

community, which is in accordance with our observation. Another study investigated the interactions among five bacterial species in a cellulose-degrading community and also found that the strains performing the last step of the cellulose degradation dominated the community (Souichiro et al., 2005). Moreover, one study investigated the dynamics of a consortium composed of two isolates from the same soil microcosms treated with the pesticide fenitrothion (Chie et al., 2009). In this MDOL consortium, the final product, methylhydroquinone, served as the common resource for the two strains. That study showed that the strain executing the last step overwhelmingly dominated the community and proposed that the co-existence of two members requires the second member to excrete enough methylhydroquinone to support the growth of another member. Therefore, privatization of the sole carbon source by the last strain may represent a common challenge when engineering microbial systems for organic compound degradation. However, the aforementioned studies constructed synthetic consortia using different species so that the inherent traits of different members in the consortia cannot be well controlled. For example, the last population may inherently grow faster than the other populations. For better application of our framework, we suggest further studies carefully control or quantify the inherent traits of different engineered strains involved in the MDOL communities.

Our model provides several avenues to stabilize MDOL communities. First, it is feasible to reduce the inherent growth rate of the last strain, which can be accomplished by either rationally engineering a slow-growing strain performing the last step or assigning more tasks (metabolic reactions) to this strain that incur higher energetic costs. Second, the ''private benefit'' of the last strain can be alleviated if the strains performing the initial steps are capable of obtaining metabolic by-products generated from the initial reactions. From this perspective, when designing a synthetic consortium engaged in MDOL for pollutant degradation, it may be useful to assign a by-product to the initial strains. Third, our results also showed that if the substrate is toxic, the microbial system will be more stable, which is consistent with the results in our previous study (Miaoxiao et al., 2022). Moreover, our results also showed that active transport of the final product (P) facilitated the stability of the MDOL communities. This finding offers another potential strategy to stabilize the engineered MDOL consortia through overexpressing the transporter of the final product of the strains involved. In summary, our results provide a quantitative way to evaluate the feasibility of applying these strategies to a specific pathway engineering, and thus should greatly assist in designing and managing related artificial microbial systems. In addition to the strategy proposed here, the previously proposed programmed ''self-lysis'' system (Lingchong et al., 2004; Spencer et al., 2017) can be introduced to the last population so that its population size can be self-regulated to enable the co-existence of different members. Moreover, the strains involved can be engineered to achieve an interdependent interaction through the exchange of essential and leaky metabolites (e.g., amino acids, vitamins), which is another potential strategy to maintain co-existence (Elin and David, 2019; Wenying et al., 2007). Notably, one recent study distributed different community members into spatially separated microcapsules, but proteins and small molecules can be freely transported among the capsules (Lin et al., 2022). Such a ''spatial partitioning'' strategy also enables the co-existence of multiple strains with different growth rates, as well as the manipulation of community structure.

Our study also has implications for our understanding of the evolution of MDOL among microorganisms. First, our results suggest that the individuals of the last population must evolve to possess a slower growth rate to maintain system stability. In this case, natural selection may not operate at the individual level (i.e., achieve the individual success of the last population) but at the community level (i.e., multi-level selection) (Charles, 2012; Craig and Maarten, 2002; Jos and Joël, 2016; Samir, 2006) to drive the evolution of MDOL communities. For example, natural communities usually undergo a standard life cycle (Diane et al., 2011; George et al., 2000; John et al., 2009; Leibold et al., 2004): (1) a random number of individuals with genotypes from a metacommunity is allocated to different local communities; (2) each local community grows independently; (3) the local communities are merged to form a new metacommunity so that the global genotypic frequencies are updated. Applying such a life cycle to a metacommunity engaged in MDOL, faster growing individuals of the population performing the last step may be favored within a local community, but this local community is not stable and accumulate less biomass than those with the slower growing last population after enough long period of local growth (stage 2). As a result, the slower growing last population, as well as the associated MDOL local communities, is favored at the higher level of metacommunity. This hypothesis may be examined using well-designed experimental evolution assays associated with the eco-evolutionary model (Jonas et al., 2012; Nuno et al., 2014) considering such a microbial life cycle. Such experiments and models can be also designed to define the suitable level of partitioning from metacommunity to local communities that enables the evolution of MDOL communities (Feilun

as five different initial ratios. The relative abundances of *P. stutzeri* AN0111ccdB or *P. stutzeri* AN0111x174 from experiments (orange, first row) and mathematical modeling (green, second row) are shown.

(B) Growth dynamics of the synthetic community composed of *P. stutzeri* AN1000, *P. stutzeri* AN0100, *P. stutzeri* AN0010, and *P. stutzeri* AN0001ccdB at eight different initial ratios. In these experiments, rhamnose concentration was set to 0.005% (n_k/m_k value equals 0.29). Each color region represents the relative abundance of each strain. The pie charts denote the community structure at the starting and end time points. Three independent replicates were performed for each condition.

(C) PCA analyses of the dynamics of the synthetic consortium composed of *P. stutzeri* AN0001ccdB at eight different initial ratios when the concentration of rhamnose was set to 0.005% (n_k/m_k value equals 0.29). The pie charts on the right denote the eight initial inoculation ratios, and the color marks are consistent with (B). The community structure data used for PCA analysis is the same as that in (B). The arrows show the direction of community succession.

(D) Naphthene degradation rate of the consortia containing *P. stutzeri* AN0001x174. The degradation rates were measured at the end of each transfer. Results of same experiments using synthetic community composed of *P. stutzeri* AN1000, *P. stutzeri* AN0100, *P. stutzeri* AN0010, and *P. stutzeri* AN0001x174 are shown in Figures S8D–S8F.

et al., 2022). Second, as we discussed above, the presence of several specific pathway features, such as substrate toxicity and by-product production, relax the constraints ensuring the stability of an MDOL community. Therefore, MDOL among different members may be easier to evolve in pathways that possess these specific features, and the beneficial mutations of the last population may again destabilize the community. For example, the mutants resistant to substrate toxicity may evolve in the last population. However, these mutants will not be selectively favored in the presence of the group-level selection, as we proposed above. This hypothesis can be examined using large-scale bioinformatic analysis. Third, the presence of spatial structure can also help maintain the evolutionary stability of an MDOL community (Craig and Maarten, 2002). Our previous study found that although the last strain generally grew more in a two-member colony engaged in MDOL, the initial strain is usually not completely excluded (Miaoxiao et al., 2022), suggesting that specific spatial organizing of a community may facilitate their co-existence. In these spatially structured environments, the interaction between the two strains would require their cells to be spatially proximal to each other (Alma Dal et al., 2020; Babak et al., 2013; Miaoxiao et al., 2020; Samay et al., 2015). Even if the cells from the last strain can obtain asymmetric "private benefit," they must be located in close proximity to their partners. Therefore, the spatial organization of an MDOL community may help maintain the co-existence of its members, thus favoring the evolution of MDOL processes. This hypothesis can be examined by comparing the results of evolutionary experiments in biofilms and well-mixed systems.

In conclusion, our results provide a basis for a theory guiding the application of MDOL strategy to design and manipulate artificial microbial systems and also provide new perspectives for understanding the evolution of natural MDOL systems.

Limitations of the study

We acknowledge several important limitations of our study. First, using the mathematical model, we simulated the assembly of the MDOL community in many different metabolic conditions (Figure 2). However, our three synthetic consortia only represent three specific cases of MDOL communities associated with the given set of metabolic conditions. The model predictions of how every single factor of metabolic conditions affects the assembly of the MDOL community has not been rigorously verified because of the limitations of the experimental setup. Second, the effects of different metabolic conditions (Figure 2) on the assembly of the multi-step MDOL communities were not discussed in this study. Finally, we knocked in two genes encoding two toxins (CcdB and phiX174 E protein) to control the death rates of the two populations in this study. Because inducing these toxins imposes a strong selection pressure on the mutations of these toxin genes, it may enable the uncontrollable fast growth of the last populations and lead to the collapse of the community. Although such mutations were not detected during the period of our experiments (three passages cycles; Figure S12), it is still possible that they may emerge if the long-term experiments were performed, which may limit the application of our method in enabling the long-term stability of an MDOL community.

STAR★METHODS

Detailed methods are provided in the online version of this paper and include the following:

- KEY RESOURCES TABLE
- RESOURCE AVAILABILITY
  - Lead contact
  - Materials availability
  - Data and code availability
- EXPERIMENTAL MODEL AND SUBJECT DETAILS
  - Construction and culturing of the synthetic microbial communities
- METHOD DETAILS
  - Formulation of the ODE models
- QUANTIFICATION AND STATISTICAL ANALYSES
  - Replication, randomization, blinding and reagent validations

SUPPLEMENTAL INFORMATION

Supplemental information can be found online at https://doi.org/10.1016/j.celrep.2022.111410.

ACKNOWLEDGMENTS

We wish to thank Professor Ping Xu (Shanghai Jiao Tong University, Shanghai, P.R. China) for supplying plasmid pMMPc-Gm, used for fluorescence labeling in this study; Dr. Min Lin (Chinese Academy of Agricultural Sciences, Beijing, P.R. China) for providing plasmid pK18mobsacB and pRK2013, used for genetic engineering in this work; Dr. T. Juelich (UCAS, Beijing) for linguistic assistance during the preparation of this manuscript. M.W. wishes to thank his most intelligent and charming wife, Yaxi Li, who provides endless inspiration for his research. This work was supported by the National Key R&D Program of China (grants 2018YFA0902100 and 2021YFA0910300), and the National Natural Science Foundation of China (grants 91951204, 31761133006, 31770120, and 31770118).

AUTHOR CONTRIBUTIONS

M.W. and Y.N. were involved in the conceptualization of the study. M.W. constructed the ODE models and performed mathematical simulations. M.W. designed the experiments. M.W., X.C., Y.F., X.Z., and T.H. performed the experiments. M.W. analyzed the data. X.L. contributed to the essential analysis methods. M.W. wrote the original draft. M.A., Y.N., and X.-L.W. edited the manuscript. Y.N., Y.-Q.T., and X.-L.W. raised the funding for the project.

DECLARATION OF INTERESTS

The authors declare no competing interests.

Received: April 14, 2022
Revised: July 10, 2022
Accepted: September 2, 2022
Published: September 27, 2022

SUPPORTING CITATIONS

The following references appear in the supplemental information: Abouseoud et al., 2010, Bar-Even et al., 2011, Brunet-Galmes et al., 2012, Camara et al., 2007, Cheffi et al., 2020, Choi and Schweizer, 2006, Dutta et al., 2017, Gorochowski et al., 2012, Harris and Theriot, 2018, Jouanneau et al., 2006, Kovarova-Kovar and Egli, 1998, Lin et al., 2010, Maier et al., 2011, Meisner and

Goldberg, 2016, Pande et al., 2016, Travisano and Lenski, 1996, Viggiani et al., 2004, Zimmerman and Trach, 1991.

REFERENCES

Abouseoud, M., Yataghene, A., Amrane, A., and Maachi, R. (2010). Effect of pH and salinity on the emulsifying capacity and naphthalene solubility of a biosurfactant produced by *Pseudomonas fluorescens*. J. Hazard Mater. *180*, 131–136.

Aiba, S., Shoda, M., and Nagatani, M. (2000). Kinetics of product inhibition in alcohol fermentation. Biotechnol. Bioeng. *67*, 671–690.

Herrero, A.A. (1983). End-product inhibition in anaerobic fermentations. Trends Biotechnol. *1*, 49–53.

Dal Co, A., van Vliet, S., Kiviet, D.J., Schlegel, S., and Ackermann, M. (2020). Short-range interactions govern the dynamics and functions of microbial communities. Nat. Ecol. Evol. *4*, 366–375.

Momeni, B., Waite, A.J., and Shou, W. (2013). Spatial self-organization favors heterotypic cooperation over cheating. Elife *2*, e00960.

Bar-Even, A., Noor, E., Savir, Y., Liebermeister, W., Davidi, D., Tawfik, D.S., and Milo, R. (2011). The moderately efficient enzyme: evolutionary and physicochemical trends shaping enzyme parameters. Biochemistry *50*, 4402–4410.

Schink, B., and Pfennig, N. (1982). Fermentation of trihydroxybenzenes by *Pelobacter acidigallici* gen. nov. sp. nov., a new strictly anaerobic, non-spore-forming bacterium. Arch. Microbiol. *133*, 195–201.

Blair, E.M., Dickson, K.L., and O'Malley, M.A. (2021). Microbial communities and their enzymes facilitate degradation of recalcitrant polymers in anaerobic digestion. Curr. Opin. Microbiol. *64*, 100–108.

Logan, B.E., and Rabaey, K. (2012). Conversion of wastes into bioelectricity and chemicals by using microbial electrochemical technologies. Science *337*, 686–690.

Brunet-Galmés, I., Busquets, A., Peña, A., Gomila, M., Nogales, B., García-Valdés, E., Lalucat, J., Bennasar, A., and Bosch, R. (2012). Complete genome sequence of the naphthalene-degrading bacterium *Pseudomonas stutzeri* AN10 (CCUG 29243). J. Bacteriol. *194*, 6642–6643.

Cámara, B., Bielecki, P., Kaminski, F., dos Santos, V.M., Plumeier, I., Nikodem, P., and Pieper, D.H. (2007). A gene cluster involved in degradation of substituted salicylates via ortho cleavage in *Pseudomonas* sp strain MT1 encodes enzymes specifically adapted for transformation of 4-methylcatechol and 3-methylmuconate. J. Bacteriol. *189*, 1664–1674.

Li, C.M., Wu, H.Z., Wang, Y.X., Zhu, S., and Wei, C.H. (2020). Enhancement of phenol biodegradation: metabolic division of labor in co-culture of *Stenotrophomonas* sp. N5 and *Advenella* sp. B9. J. Hazard Mater. *400*, 123214.

Gao, C., Wang, Y., Zhang, Y., Lv, M., Dou, P., Xu, P., and Ma, C. (2015). NAD-independent l-Lactate dehydrogenase required for l-Lactate utilization in *Pseudomonas stutzeri* A1501. J. Bacteriol. *197*, 2239–2247.

Goodnight, C. (2012). On multilevel selection and kin selection : contextual analysis meets direct fitness. Evolution *67*, 1539–1548.

Cheffi, M., Hentati, D., Chebbi, A., Mhiri, N., Sayadi, S., Marqués, A.M., and Chamkha, M. (2020). Isolation and characterization of a newly naphthalene-degrading *Halomonas pacifica*, strain Cnaph3: biodegradation and biosurfactant production studies. 3 Biotech *10*, 89.

Chi Kyu, A., Seung Han, W., Dae Sung, L., and Jong Moon, P. (2006). Mathematical evaluation of intermediates accumulation during microbial phenanthrene degradation. Korean Journal of Chemical Engineering *23*, 415–418.

Chie, K., Nakaoka, S., Takeuchi, Y., Tago, K., Hayatsu, M., and Kato, K. (2009). Complementary cooperation between two syntrophic bacteria in pesticide degradation. J. Theor. Biol. *256*, 644–654.

Choi, K.H., and Schweizer, H.P. (2006). mini-Tn7 insertion in bacteria with single attTn7 sites: example *Pseudomonas aeruginosa*. Nat. Protoc. *1*, 153–161.

Wang, C., Huang, Y., Zhang, Z., Hao, H., and Wang, H. (2020). Absence of the nahG -like gene caused the syntrophic interaction between Marinobacter and other microbes in PAH -degrading process. J. Hazard Mater. *384*, 121387.

Johnson, C.R., and Boerlijst, M.C. (2002). Selection at the level of the community: the importance of spatial structure. Trends Ecol. Evol. *17*, 83–90.

David, A.R. (2012). The human microbiome: ecosystem resilience and health. Nutr. Rev. *70*, S2–S9.

Ghosal, D., Ghosh, S., Dutta, T.K., and Ahn, Y. (2016). Current state of knowledge in microbial degradation of polycyclic aromatic hydrocarbons (PAHs): a review. Front. Microbiol. *7*, 1369.

Diane, M., Scott, A.R., Nicolas, B., Peter, D.S., and Staffan, K. (2011). Should we stay or should we go: mechanisms and ecological consequences for biofilm dispersal. Nat. Rev. Microbiol. *10*, 39–50.

Doron, L., Raab, N., Pinto, Y., Rothschild, D., Zanir, G., Godneva, A., Mellul, N., Futorian, D., Gal, D., Leviatan, S., et al. (2021). Diversity and functional landscapes in the microbiota of animals in the wild. Science *372*, eabb5352.

Dutta, K., Shityakov, S., Das, P.P., and Ghosh, C. (2017). Enhanced biodegradation of mixed PAHs by mutated naphthalene 1, 2-dioxygenase encoded by *Pseudomonas putida* strain KD6 isolated from petroleum refinery waste. 3 Biotech *7*, 365.

Elin, E.L., and David, R.J. (2019). Substrate cross-feeding affects the speed and trajectory of molecular evolution within a synthetic microbial assemblage. BMC Evol. Biol. *19*, 129.

Elizabeth, M.A., Flynn, J., Hunter, R.C., and Harcombe, W.R. (2018). Cross-feeding modulates antibiotic tolerance in bacterial communities. ISME J. *12*, 2723–2735.

Graham, E.B., Knelman, J.E., Schindlbacher, A., Siciliano, S., Breulmann, M., Yannarell, A., Beman, J.M., Abell, G., Philippot, L., Prosser, J., et al. (2016). Microbes as engines of ecosystem function: when does community structure enhance predictions of ecosystem processes? Front. Microbiol. *7*, 214.

Emily, H., Heys, J., and Gedeon, T. (2014). Quantifying the effects of the division of labor in metabolic pathways. J. Theor. Biol. *360*, 222–242.

Eulyn, P., Vassileva, K., Mills, C.G., Bush, T., Blythe, R.A., Schwarz-Linek, J., Strathdee, F., Allen, R.J., and Free, A. (2017). Assembly of microbial communities in replicate nutrient-cycling model ecosystems follows divergent trajectories, leading to alternate stable states. Environ. Microbiol. *19*, 3374–3386.

Feilun, W., Yuanchi, H., Andrea, W., Meidi, W., Jeffrey, L., Shangying, W., Nan, L., Shuquan, H., Charlotte, T.L., Lawrence, A.D., et al. (2022). Modulation of microbial community dynamics by spatial partitioning. Nat. Chem. Biol. *18*, 394–402.

Flint, H.J., Scott, K.P., Louis, P., and Duncan, S.H. (2012). The role of the gut microbiota in nutrition and health. Nat. Rev. Gastroenterol. Hepatol. *9*, 577–589.

George, O., Kaplan, H.B., and Kolter, R. (2000). Biofilm formation as microbial development. Annu. Rev. Microbiol. *54*, 49–79.

Gilbert, E.S., Walker, A.W., and Keasling, J.D. (2003). A constructed microbial consortium for biodegradation of the organophosphorus insecticide parathion. Appl. Microbiol. Biotechnol. *61*, 77–81.

Gorochowski, T.E., Matyjaszkiewicz, A., Todd, T., Oak, N., Kowalska, K., Reid, S., Tsaneva-Atanasova, K.T., Savery, N.J., Grierson, C.S., and di Bernardo, M. (2012). BSim: an agent-based tool for modeling bacterial populations in systems and synthetic biology. PLoS One *7*, e42790.

Pumphrey, G.M., and Madsen, E.L. (2007). Naphthalene metabolism and growth inhibition by naphthalene in Polaromonas naphthalenivorans strain CJ 2. Microbiology *153*, 3730–3738.

Greg, P.M., Bernt, C.M., and Butler, A. (2018). Catechol oxidation: considerations in the design of wet adhesive materials. Biomater. Sci. *6*, 332–339.

Hao, Z., Perreau, J., Powell, J.E., Han, B., Zhang, Z., Kwong, W.K., Tringe, S.G., and Moran, N.A. (2019). Division of labor in honey bee gut microbiota for plant polysaccharide digestion. Proc. Natl. Acad. Sci. USA *116*, 25909–25916.

Harris, L.K., and Theriot, J.A. (2018). Surface area to volume ratio: a natural variable for bacterial morphogenesis. Trends Microbiol. *26*, 815–832.

Henrich, B., Lubitz, W., and Plapp, R. (1982). Lysis of Escherichia coli by induction of cloned *φX174* genes. Mol. Gen. Genet. *185*, 493–497.

Ian, M.H., Jones, D.M., and Larter, S.R. (2003). Biological activity in the deep subsurface and the origin of heavy oil. Nature *426*, 344–352.

Brunet-Galmés, I., Busquets, A., Peña, A., Gomila, M., Nogales, B., García-Valdés, E., Lalucat, J., Bennasar, A., and Bosch, R. (2012). Complete genome sequence of the naphthalene-degrading bacterium Pseudomonas stutzeri AN10 (CCUG 29243). J. Bacteriol. *194*, 6642–6643.

Jan-Ulrich, K., Benjamin, M.G., and Rebeca, G.-C. (2020). Evolutionary causes and consequences of metabolic division of labour: why anaerobes do and aerobes don't. Curr. Opin. Biotechnol. *62*, 80–87.

Jed, A.F. (2009). Microbial community structure and its functional implications. Nature *459*, 193–199.

Jie-Liang, L., Yong, N., Miaoxiao, W., Guangming, X., Yi-Ping, W., Edmund, M., and Xiao-Lei, W. (2015). Regulation of alkane degradation pathway by a TetR family repressor via an autoregulation positive feedback mechanism in a Gram-positive *Dietzia* bacterium. Mol. Microbiol. *99*, 338–359.

Bing, H., Jan, D., Yan, L., Yue-Qin, T., Yiming, J., Chang-Qiao, C., Jianmin, X., Yong, N., and Xiao-Lei, W. (2021). Thermodynamically favorable reactions shape the archaeal community affecting bacterial community assembly in oil reservoirs. Sci. Total Environ. *781*, 146506.

John, S.C., Olivier, R., and Stanislas, L. (2009). Simpson's paradox in a synthetic microbial system. Science *323*, 272–275.

Jonas, C., Anna, M., and Erwin, F. (2012). Growth dynamics and the evolution of cooperation in microbial populations. Sci. Rep. *2*, 281.

Jonathan, F., Logan, M.H., and Jeff, G. (2017). Community structure follows simple assembly rules in microbial microcosms. Nat. Ecol. Evol. *1*, 109.

Jonathan, M.C. (2003). Community assembly: when should history matter? Oecologia *136*, 489–498.

Jones, J.A., Vernacchio, V.R., Collins, S.M., Shirke, A.N., Xiu, Y., Englaender, J.A., Cress, B.F., McCutcheon, C.C., Linhardt, R.J., Gross, R.A., and Koffas, M.A.G. (2017). Complete biosynthesis of anthocyanins using E. coli polycultures. mBio *8*. e00621-17.

Jos, K., and Joël, M. (2016). Kin and multilevel selection in social evolution: a never-ending controversy? F1000Res. *5*, 776.

Jouanneau, Y., Meyer, C., Jakoncic, J., Stojanoff, V., and Gaillard, J. (2006). Characterization of a naphthalene dioxygenase endowed with an exceptionally broad substrate specificity toward polycyclic aromatic hydrocarbons. Biochemistry *45*, 12380–12391.

Kovarova-Kovar, K., and Egli, T. (1998). Growth kinetics of suspended microbial cells: from single-substrate-controlled growth to mixed-substrate kinetics. Microbiol. Mol. Biol. Rev. *62*, 646–666.

Leibold, M.A., Holyoak, M., Mouquet, N., Amarasekare, P., Chase, J.M., Hoopes, M.F., Holt, R.D., Shurin, J.B., Law, R., Tilman, D., et al. (2004). The metacommunity concept: a framework for multi-scale community ecology. Ecol. Lett. *7*, 601–613.

Lin, C., Gan, L., and Chen, Z.L. (2010). Biodegradation of naphthalene by strain *Bacillus fusiformis* (BFN). J. Hazard Mater. *182*, 771–777.

Lin, W., Xi, Z., Chenwang, T., Pengcheng, L., Runtao, Z., Jing, S., Yunfeng, Z., Hua, C., Jiajia, M., Xinyu, S., et al. (2022). Engineering consortia by polymeric microbial swarmbots. Nat Commun *13*.

Lingchong, Y., Robert Sidney, C., Ron, W., and Frances, H.A. (2004). Programmed population control by cell–cell communication and regulated killing. Nature *428*, 868–871.

Lori, N., Ian, B., Minghao, L., Kevin, C., David, F., Catherine, H., Kaitlin, C., Suyen Espinoza, M., Samantha, D., Matthew, C., et al. (2019). Microbial coexistence through chemical-mediated interactions. Nat. Commun. *10*, 2052.

Maier, T., Schmidt, A., Güell, M., Kühner, S., Gavin, A.C., Aebersold, R., and Serrano, L. (2011). Quantification of mRNA and protein and integration with protein turnover in a bacterium. Mol. Syst. Biol. *7*, 511.

Manuel, D.-B., Oliverio, A.M., Brewer, T.E., Benavent-González, A., Eldridge, D.J., Bardgett, R.D., Maestre, F.T., Singh, B.K., and Fierer, N. (2018). A global atlas of the dominant bacteria found in soil. Science *359*, 320–325.

Mariana, P.L., Christie-Oleza, J.A., Martín-Cardona, C., Suárez-Suárez, L.Y., Lalucat, J., Nogales, B., and Bosch, R. (2009). Physiological role of NahW, the additional salicylate hydroxylase found in *Pseudomonas stutzeri* AN10. FEMS Microbiol. Lett. *300*, 265–272.

Meghan, T., Taiyao, W., Qi, Z., Ioannis, C.P., and Daniel, S. (2019). Designing metabolic division of labor in microbial communities. mSystems *4*. e00263-18.

Meisner, J., and Goldberg, J.B. (2016). The *Escherichia coli* rhaSR-PrhaBAD inducible promoter system Allows tightly controlled gene expression over a wide range in *Pseudomonas aeruginosa*. Appl. Environ. Microbiol. *82*, 6715–6727.

Miaoxiao, W., Chen, X., Tang, Y., Nie, Y., and Wu, X. (2022). Substrate availability and toxicity shape the structure of microbial communities engaged in metabolic division of labor. mLife *1*, 131–145.

Miaoxiao, W., Liu, X., Nie, Y., and Wu, X.L. (2020). Selfishness driving reductive evolution shapes interdependent patterns in spatially structured microbial communities. The ISME Journal *15*, 1387–1401.

Minh-Hoa, D.-T., Van Melderen, L., De Genst, E., Afif, H., Buts, L., Wyns, L., and Loris, R. (2005). Molecular basis of gyrase poisoning by the addiction toxin CcdB. J. Mol. Biol. *348*, 1091–1102.

Muoz, R., Daz, L.F., Bordel, S., and Villaverde, S. (2007). Inhibitory effects of catechol accumulation on benzene biodegradation in *Pseudomonas putida* F1 cultures. Chemosphere *68*, 244–252.

Nicole, J.Y., and Marlon, J.H. (2014). Getting across the Cell Membrane: An Overview for Small Molecules, Peptides, and Proteins (Springer).

Nina, D., Donaho, J.A., Gutierrez, T., Seitz, K.W., Teske, A.P., and Baker, B.J. (2016). Reconstructing metabolic pathways of hydrocarbon-degrading bacteria from the Deepwater Horizon oil spill. Nat. Microbiol. *1*, 16057.

Nuno, M.O., Rene, N., and Kevin, R.F. (2014). Evolutionary limits to cooperation in microbial communities. Proc. Natl. Acad. Sci. USA *111*, 17941–17946.

Ori, F., Liat, S., Goor, S., Fotini, K., Hen, H., Shamay, J., Tomer, H., Otto, X.C., Eran, H., and Itzhak, M. (2020). Stochasticity constrained by deterministic effects of diet and age drive rumen microbiome assembly dynamics. Nat. Commun. *11*, 1904.

Pablo, M.A., Luca, I.C.d.F., and Hiplito, F.P. (2020). Application of Microbial Consortia in Degradation and Detoxification of Industrial Pollutants (Elsevier).

Pande, S., Kaftan, F., Lang, S., Svatoš, A., Germerodt, S., and Kost, C. (2016). Privatization of cooperative benefits stabilizes mutualistic cross-feeding interactions in spatially structured environments. ISME J. *10*, 1413–1423.

Park, W., Jeon, C.O., Cadillo, H., DeRito, C., and Madsen, E.L. (2004). Survival of naphthalene-degrading Pseudomonas putida NCIB 9816-4 in naphthalene-amended soils: toxicity of naphthalene and its metabolites. Appl. Microbiol. Biotechnol. *64*, 429–435.

Paul, G.F., Tom, F., and Edward, F.D. (2008). The microbial engines that drive earth's biogeochemical cycles. Science *320*, 1034–1039.

Rafael, B., Elena, G.-V., and Edward, R.B.M. (1999). Genetic characterization and evolutionary implications of a chromosomally encoded naphthalene-degradation upper pathway from *Pseudomonas stutzeri* AN10. Gene *236*, 149–157.

Rafael, B., Elena, G.-V., and Edward, R.B.M. (2000). Complete nucleotide sequence and evolutionary significance of a chromosomally encoded naphthalene-degradation lower pathway from *Pseudomonas stutzeri* AN10. Gene *245*, 65–74.

Robin, T., and Dani, O. (2017). Cooperation in carbon source degradation shapes spatial self-organization of microbial consortia on hydrated surfaces. Sci. Rep. *7*, 43726.

Ryan, T., Feilun, W., Carolyn, Z., Sharon, B., David, K., and Lingchong, Y. (2018). Metabolic division of labor in microbial systems. Proc. Natl. Acad. Sci. USA *115*, 2526–2531.

Samay, P., Filip, K., Stefan, L., Ale, S., Sebastian, G., and Christian, K. (2015). Privatization of cooperative benefits stabilizes mutualistic cross-feeding interactions in spatially structured environments. ISME J. *10*, 1413–1423.

Samir, O. (2006). Evolution and the Levels of Selection (Oxford University Press).

Shalini, G., Bhawana, P., and Fulekar, M.H. (2014). Molecular approaches for biodegradation of polycyclic aromatic hydrocarbon compounds: a review. Rev. Environ. Sci. Biotechnol. *14*, 241–269.

Souichiro, K., Shin, H., Zong Jun, C., Masaharu, I., and Yasuo, I. (2005). Stable coexistence of five bacterial strains as a cellulose-degrading community. Appl. Environ. Microbiol. *71*, 7099–7106.

Spencer, R.S., Din, M.O., Philip, B., Liyang, X., Lev, S.T., and Jeff, H. (2017). A stabilized microbial ecosystem of self-limiting bacteria using synthetic quorum-regulated lysis. Nat. Microbiol. *2*, 17083.

Tadashi, F. (2015). Historical contingency in community assembly: integrating niches, species pools, and priority effects. Annu. Rev. Ecol. Evol. Syst. *46*, 1–23.

Thompson, L.R., Sanders, J.G., McDonald, D., Amir, A., Ladau, J., Locey, K.J., Prill, R.J., Tripathi, A., Gibbons, S.M., Ackermann, G., et al. (2017). A communal catalogue reveals Earth's multiscale microbial diversity. Nature *551*, 457–463.

Travisano, M., and Lenski, R.E. (1996). Long-term experimental evolution in Escherichia coli .4. Targets of selection and the specificity of adaptation. Genetics *143*, 15–26.

Viggiani, A., Siani, L., Notomista, E., Birolo, L., Pucci, P., and Di Donato, A. (2004). The role of the conserved residues His-246, His-199, and Tyr-255 in the catalysis of catechol 2, 3-dioxygenase from Pseudomonas stutzeri OX1. J. Biol. Chem. *279*, 48630–48639.

Wenying, S., Sri, R., and Jose, M.G.V. (2007). Synthetic cooperation in engineered yeast populations. Proc. Natl. Acad. Sci. USA *104*, 1877–1882.

Xiaoqiang, J., Yun, H., Dawei, J., Chang, L., and Wenyu, L. (2019). Construction and analysis of an engineered *Escherichia coli-Pseudomonas aeruginosa* co-culture consortium for phenanthrene bioremoval. Biochem. Eng. J. *148*, 214–223.

Xuefeng, P., St. Elmo, W., Thomas, S.L., Sean, P.G., Jennifer, L.B., John, K.H., Candice, L.S., Asaf, S., Kerrie, B., Igor, V.G., et al. (2021). Genomic and functional analyses of fungal and bacterial consortia that enable lignocellulose breakdown in goat gut microbiomes. Nat. Microbiol. *6*, 499–511.

Youqiang, X., Fei, T., Cuiqing, M., and Ping, X. (2013). New constitutive vectors: useful genetic engineering tools for biocatalysis. Appl. Environ. Microbiol. *79*, 2836–2840.

Zimmerman, S.B., and Trach, S.O. (1991). Estimation of macromolecule concentrations and excluded volume effects for the cytoplasm of *Escherichia coli*. J. Mol. Biol. *222*, 599–620.

STAR★METHODS

KEY RESOURCES TABLE

REAGENT or RESOURCE	SOURCE	IDENTIFIER
Bacterial and virus strains		
See Table S3	N/A	N/A
Chemicals, peptides, and recombinant proteins		
EcoRI	Takara	Cat# 1040A
HindIII	Takara	Cat# 1060A
T4 DNA Ligase	Takara	Cat# 2011B
Phanta® Max Super-Fidelity DNA Polymerase	Vazyme	Cat# P505-d1
Rapid Taq Master Mix	Vazyme	Cat# P222-03
YeaRed Nucleic Acid Gel Stain (10,000× in Water)	Yeasen	Cat# 10202ES76
Sucrose	Sigma-Aldrich	Cat# S0389
Kanamycin sulfate	Sigma-Aldrich	Cat# K1377
Gentamicin sulfate salt	Sigma-Aldrich	Cat# G1264
Nalidixic acid	Sigma-Aldrich	Cat# N8878
IPTG	Sigma-Aldrich	Cat# I6758
L-Rhamnose	Sigma-Aldrich	Cat# W373011
Naphthalene	Sigma-Aldrich	Cat# 84679
1,2-dihydroxynaphthalene (1,2-DHN)	Sigma-Aldrich	Cat# 232505
Sodium Salicylate	Sigma-Aldrich	Cat# S3007
Pyrocatechol	Sigma-Aldrich	Cat# C9510
Sodium pyruvate	Sigma-Aldrich	Cat# P2256
Critical commercial assays		
FastPure Bacteria DNA Isolation Mini Kit	Vazyme	Cat# DC103
EasyPure® Plasmid MiniPrep Kit	TransGen Biotech	Cat# EM101-01
EasyPure® Quick Gel Extraction Kit	TransGen Biotech	Cat# EG101-01
EasyPure® PCR Purification Kit	TransGen Biotech	Cat# EP101-01
Hieff Clone® Plus Multi One Step Cloning Kit	Yeasen	Cat# 10912ES10
Deposited data		
Raw data of coculture	This paper	Miaoxiao et al. (2022), "MDOL paper dataset", Mendeley Data, V1, https://doi.org/10.17632/r58wvpdhb3.1
The detailed protocols for mathematical modeling, construction of the synthetic consortia, and co-culture experiments.	This paper	Miaoxiao et al. (2022), "MDOL paper supplementary materials", Mendeley Data, V1, https://doi.org/10.17632/87ctyv6chg.1
Experimental models: Organisms/strains		
P. stutzeri: Strain background: AN10	Brunet-Galmes, I. et al. 2012	N/A
All strains used in this study can be found in Table S3.	This paper	N/A
Oligonucleotides		
Primers used in this study	This paper	Wang, Miaoxiao et al. (2022), "MDOL paper dataset", Mendeley Data, V1, https://doi.org/10.17632/r58wvpdhb3.1
Recombinant DNA		
Plasmids for fluorescent labeling, see Table S6.	This paper	N/A
Plasmids for constructing the ccdB and phiX174 E genetic modules, see Table S6.	This paper	N/A

(*Continued on next page*)

Continued

REAGENT or RESOURCE	SOURCE	IDENTIFIER
Software and algorithms		
Wolfram Mathematica	Wolfram Research	Version 12.3
SnapGene	Dotmatics	https://www.snapgene.com/
Other		
The source codes used for the mathematical modeling in this study	This paper	Wang, Miaoxiao et al. (2022), "MDOL paper-simulation code", Mendeley Data, V1, https://doi.org/10.17632/rbn7cwb4hn.1

RESOURCE AVAILABILITY

Lead contact

Further information and requests for resources and reagents can be made to the Lead Contact, Xiao-Lei Wu, xiaolei_wu@pku.edu.cn.

Materials availability

Requests for plasmids and strains described in this study can be made to the lead contact, Xiao-Lei Wu, xiaolei_wu@pku.edu.cn.

Data and code availability

Raw data of coculture and mathematical simulations are available on Mendeley Data: Wang, Miaoxiao et al. (2022), "MDOL paper dataset", Mendeley Data, V1, https://doi.org/10.17632/r58wvpdhb3.1. The source codes used for all the models concerning are publicly available (Mendeley Data, https://doi.org/10.17632/rbn7cwb4hn.1). The detailed derivations of all models, justifications of our assumptions, and the detailed protocols of the construction and culturing of our synthetic microbial communities are publicly available on (Mendeley Data, https://doi.org/10.17632/87ctyv6chg.1). Any additional information required to reanalyze the data reported in this paper is available from the lead contact upon request.

EXPERIMENTAL MODEL AND SUBJECT DETAILS

Construction and culturing of the synthetic microbial communities

Construction of the strains involved in the synthetic microbial communities

The strains and plasmids used in this study are summarized in Table S3. All *P. stutzeri* strains were engineered from a naphthalene-degrading bacterial strain *P. stutzeri* AN10 (Isabel et al., 2012; Rafael et al., 2000). Genes that encode the key enzymes responsible for the four metabolic steps in the naphthalene degradation pathway were knocked out to generate different strains involved in the synthetic microbial consortia. The details of the strain design and construction are described in the publicly available Supplementary file (Mendeley Data, https://doi.org/10.17632/87ctyv6chg.1). To label the strains with fluorescence for the measurement of their relative abundance in synthetic consortia, *eCFP*, *dsRed*, *mBeRFP*, *mCherry*, or *eGFP* gene was cloned into a constitutive vector, pMMPc-Gm (Youqiang et al., 2013), and delivered to the host cells via triparental filter mating (Chao et al., 2015).

Culturing of the synthetic microbial communities

Our synthetic microbial communities were cultured in 25-mL flasks containing 5 mL new fresh minimum medium (Jie-Liang et al., 2015) supplemented with naphthalene powder (1% w/v) as the sole carbon source. The biomass and relative fraction were measured using the method described previously (Elizabeth et al., 2018; Miaoxiao et al., 2022). The detailed protocols were described in the publicly available Supplementary file (Mendeley Data, https://doi.org/10.17632/87ctyv6chg.1).

METHOD DETAILS

Formulation of the ODE models

The mathematical models were built using ordinary differential equations, which formulated the dynamics of intracellular and extracellular intermediates and end products, as well as the growth of all the strains involved in the community. In all cases, the models were built on a well-mixed system (or sufficiently fast metabolite diffusion). Here, the dimensionless forms of the models were presented. The detailed derivations of all models and justifications of our assumptions are described in the publicly available Supplementary file (Mendeley Data, https://doi.org/10.17632/87ctyv6chg.1). The definitions and dimensionless methods of all the variables and parameters are listed in Tables S1 and S2.

The basic ODE models for a two-step MDOL community

As described in the first part of the Results section, we assumed that a two-step pathway was implemented by MDOL between two strains (Figure S1A). Details about the construction of this basic ODE system are described in the publicly available Supplementary file (Mendeley Data, https://doi.org/10.17632/87ctyv6chg.1). For simplicity, the basic model was built based on seven simple

assumptions, namely transport via passive diffusion, intracellular metabolic reactions, negligible abiotic degradation of I and P, excess of initial substrate, as well as low levels of intracellular accumulation of I and P; importantly, P was assumed to be the sole and limited resource for the growth of the two strains and its consumption was calculated following Monod equations. Thus, the dynamics of intracellular and extracellular I and P are given by

$$\frac{di_{1,in}}{d\tau} = a_1 - \gamma_i \cdot (i_{1,in} - i_{out}) \quad \text{(Equation 8)}$$

$$\frac{di_{2,in}}{d\tau} = -a_2 i_{2,in} + \gamma_i \cdot (i_{out} - i_{2,in}) \quad \text{(Equation 9)}$$

$$\frac{dp_{1,in}}{d\tau} = -lg_1 p_{1,in} + \gamma_p \cdot (p_{out} - p_{1,in}) \quad \text{(Equation 10)}$$

$$\frac{dp_{2,in}}{d\tau} = a_2 i_{2,in} - lg_2 p_{2,in} - \gamma_p \cdot (p_{2,in} - p_{out}) \quad \text{(Equation 11)}$$

$$\frac{di_{out}}{d\tau} = x_1 \cdot \gamma_i \cdot (i_{1,in} - i_{out}) - x_2 \cdot \gamma_i \cdot (i_{out} - i_{2,in}) \quad \text{(Equation 12)}$$

$$\frac{dp_{out}}{d\tau} = x_2 \cdot \gamma_p \cdot (p_{2,in} - p_{out}) - x_1 \cdot \gamma_p \cdot (p_{out} - p_{1,in}) \quad \text{(Equation 13)}$$

Here, $i_{1,in}$ and $i_{2,in}$ represent the intracellular I concentration of two strains; i_{out} is the extracellular concentration of I; p_{out} is the extracellular concentration of P; $p_{1,in}$ and $p_{2,in}$ are the intracellular P concentration of two strains; x_1 and x_2 are the biomass of two strains; a_1 and a_2 are the reaction rates of two reactions; γ_i and γ_P are the diffusion rates of I and P across the cell membrane; lg_1 and lg_2 are the consumption rate of the product for the growth of two strains. The growth of the two strains was modeled using a generalized logistic function with first-order cell death:

$$\frac{dx_1}{d\tau} = \mu_1 x_1 \left(1 - \frac{x_1 + x_2}{\rho}\right) - d_1 x_1 \quad \text{(Equation 14)}$$

$$\frac{dx_2}{d\tau} = \mu_2 x_2 \left(1 - \frac{x_1 + x_2}{\rho}\right) - d_2 x_2 \quad \text{(Equation 15)}$$

Here, ρ represents the carrying capacity of the whole community; d_1 and d_2 represent the apparent maintenance rates of the two strains. The specific growth rates of the two strains, μ_1 and μ_2, are calculated by

$$\mu_1 = lg_1 p_{1,in} y_1 c_1 \quad \text{(Equation 16)}$$

$$\mu_2 = lg_2 p_{2,in} y_2 c_2 \quad \text{(Equation 17)}$$

Equations (16) and (17) are linked with our basic assumption that P is the sole resource for growth. In addition, y_1 and y_2 represent the yield coefficients for biomass production of the two strains; coefficients c_1 and c_2 are used to describe the metabolic burdens of the two reactions.

The ODE models considering complex pathway mechanisms

The models that consider the complex pathway mechanisms were built by modifying or adding the related mathematical terms to the basic model. Details of these modifications are described in the publicly available Supplementary file (Mendeley Data, https://doi.org/10.17632/87ctyv6chg.1).

The ODE models for multiple-step MDOL community

Assuming that a metabolic pathway is segregated into *N* steps that are executed by *N* strains (Figure S1A), more generalized models are built by expanding the basic framework of the two-step MDOL community, which was described in the publicly available Supplementary file (Mendeley Data, https://doi.org/10.17632/87ctyv6chg.1) in detail. In this system, an organic substrate (S) is converted

to a final product (P) through a long metabolic pathway containing *N* reactions and *N*-1 intermediate metabolites (I). Each reaction is carried out by one strain by expressing a specific enzyme. The ODE model was built accordingly,

$$\frac{di^1_{k,in}}{d\tau} = \epsilon_{k,1}a_1 - \epsilon_{k,2}a_2 \cdot i^1_{k,in} + \gamma_{i^1} \cdot \left(i^1_{out} - i^1_{k,in}\right) \quad \text{(Equation 18)}$$

$$\frac{di^j_{k,in}}{d\tau} = \epsilon_{k,j}a_k \cdot i^{j-1}_{k,in} - \epsilon_{k,j+1}a_{k+1} \cdot i^j_{k,in} + \gamma_{ij} \cdot \left(i^j_{out} - i^j_{k,in}\right), \quad (j > 1) \quad \text{(Equation 19)}$$

$$\frac{dp_{k,in}}{d\tau} = \epsilon_{k,N}a_N \cdot i^{N-1}_{k,in} - lg_k \cdot p_{k,in} + \gamma_p \cdot \left(p_{out} - p_{k,in}\right) \quad \text{(Equation 20)}$$

$$\frac{di^j_{out}}{d\tau} = -\sum_{k=1}^{N} x_k \cdot \gamma_{ij} \cdot \left(i^j_{out} - i^j_{k,in}\right) \quad \text{(Equation 21)}$$

$$\frac{dp_{out}}{d\tau} = -\sum_{k=1}^{N} x_k \cdot \gamma_p \cdot \left(p_{out} - p_{k,in}\right) \quad \text{(Equation 22)}$$

$$\frac{dx_k}{d\tau} = lg_k p_{k,in} y_k c_k x_k \left(1 - \frac{\sum_{k=1}^{N} x_k}{\rho}\right) - d_k x_k \quad \text{(Equation 23)}$$

In the model, $i^j_{k,in}$ represents the intracellular concentration of the *j*th intermediate of the *k*th strain; i^j_{out} represents the extracellular concentration of the *j*th intermediate; $p_{k,in}$ represents the intracellular P concentration of the *k*th strain; ϵ_k represents a vector that characterizes the phenotype of the *k*th strain, where ϵ_k equals $[0, 0, \ldots, 1, \ldots 0, 0]$ denoting that the *k*th strain is only capable of performing the *k*th reaction; x_k is the biomass of the *k*th strain; a_k is the reaction rates of the *k*th reactions; γ_{ij} and γ_P are the diffusion rates of the *j*th intermediate and P across the cell membrane; lg_k are the consumption rate of P of the *k*th strain; ρ is the carrying capacity of the whole communities; d_k is apparent maintenance rate of the *k*th strain; y_k is the yield coefficients for biomass production of the *k*th strain; c_k is the metabolic burdens of the *k*th strain.

The ODE model used to predict the assembly of our synthetic consortia

The models used to predict the assembly of the three 2-step MDOL synthetic consortia, as well as the four-step MDOL synthetic consortium, were built by adding the specific mechanisms of each consortium to our basic ODE model. These effects include the toxicity of the naphthalene and the intermediates, the abiotic conversion of the intermediates, and the generation of metabolic by-products in the step of converting 1, 2-hydroxynaphthalene to salicylate. In addition, the parameters, such as the reaction rates, and the consuming rate of P, were experimentally measured or obtained from previous reports. Specifically, the value of d_2 (2-step consortia) and d_4 (four-step consortia) are estimated by the experimentally fitted function that links the death rate to the rhamnose concentration. Details of the formulation of these predicting models are described in the publicly available Supplementary file (Mendeley Data, https://doi.org/10.17632/87ctyv6chg.1), and the values and sources of all the parameters used in the predicting models are listed in Table S4.

Model derivation and simulation protocols

Solving and simplifying the ODE models were performed using the Solve, Dsolve, and Simplify functions of *Wolfram Mathematica* (version 12.0), associated with the manual arrangement. In order to perform sensitivity analyses of the basic model, as well as solve those ODE systems that cannot be easily managed using a simple analytic method, numeric simulations were performed using basic settings of the NDsolve function of *Wolfram Mathematica*. The details of these model deviations are publicly available (Mendeley Data, https://doi.org/10.17632/87ctyv6chg.1), Including: (1) the derivation methods of the basic assembly rule of a two-step MDOL community (see Equations (1) and (2)); (2) Analyses of the models considering those complex mechanisms; (3) Derivation methods of the assembly rule of multiple-step MDOL community (that is, Equations (3), (4), and (5)); (4) Simulation protocols and parameterization of the models for predicting experimental results; (5) Simulation protocols that test the effects of initial strain ratio on the assembly rule. These analyses were performed using custom *Wolfram Mathematica* scripts. The generated data were then analyzed and visualized using basic functions in *Wolfram Mathematica*, of which the custom codes were integrated into the aforementioned scripts.

QUANTIFICATION AND STATISTICAL ANALYSES

The statistical methods are described in figure legends. To fit the simulation or experimental data with the proposed function, LinearModelFit function in *Wolfram Mathematica* (version 12.0) was used for linear fit, while the NonlinearModelFit function was used for non-linear fit with the default settings, both with default settings. The values of adjusted R-squared can be found in all related figures.

Replication, randomization, blinding and reagent validations

Replicate experiments have been performed for all key data shown in this study. Biological or technical replicate samples were randomized where appropriate. The numbers of replicates are listed in the related figure legends.